AD-A256 612

DTIC
ELECTE
OCT 2 7 1992
S
C

THE DETECTION AND CORRELATION
MODELING OF RAYLEIGH DISTRIBUTED
RADAR SIGNALS

THESIS

Alan Lee Buterbaugh
Captain, USAF

92-28125

AFIT/GE/ENG/92S-03

THE DETECTION AND CORRELATION
MODELING OF RAYLEIGH DISTRIBUTED
RADAR SIGNALS

THESIS

Presented to the Faculty of the School of Engineering

of the Air Force Institute of Technology

Air University

In Partial Fulfillment of the

Requirements for the Degree of

Master of Science in Electrical Engineering

Alan Lee Buterbaugh, B.S.

Captain, USAF

September, 1992

Acknowledgements

I want to thank my thesis advisor Dr Byron M. Welsh for his guidance during this thesis project. I also want to thank the members of the 6585 Test Group, Radar Target Scattering Division, for suggesting this topic and providing the financial resources necessary to complete this thesis.

I am grateful to my classmates for their friendship and help throughout our many classes. I am especially grateful to my wife Alicia who supported me every way she possibly could throughout the thesis effort.

<div align="right">Alan L. Buterbaugh</div>

Table of Contents

List of Figures

List of Tables

AFIT/GE/ENG/92S-03

Abstract

This thesis provides a method for determining the detection of partially correlated Rayleigh distributed radar returns by a pulsed search radar. The receiver consists of a quadrature demodulator receiver, followed by a square law envelope detector and a linear post-detection integrator. In addition, a technique for determining the pulse-to-pulse correlation of a complex target is given using inverse Fourier transforms of the target scattering centers. An AIM-9 missile is used to illustrate how the partially correlated detection techniques and the pulse-to-pulse correlation predictions can be used to determine the probability of detection.

THE DETECTION AND CORRELATION
MODELING OF RAYLEIGH DISTRIBUTED
RADAR SIGNALS

I. Introduction

1.1 Background

One of the major areas of interest in the development of military aircraft systems is the radar power reflected or scattered from an aircraft when it is illuminated by a radar. The measure of this scattered power is called the radar cross section (RCS). The RCS of an aircraft is typically measured in $0.1°$ azimuth samples for a given elevation angle. At radar frequencies greater than 8 GHz the highly fluctuating RCS may be under-sampled and an accurate characterization of the RCS may not be achieved. Increasing the angular sampling rate will give a more detailed characterization of the RCS; however, the cost required to upgrade the measurement systems to achieve the smaller angular samples is high. The additional information obtained from improved sampling may be of marginal value when compared to the price required to upgrade the measurement system.

If we are interested in an exact deterministic characterization of the target's RCS, then we would nominally need a sampling rate to support at least two samples for every lobe. This criteria is impossible to achieve for complex targets due to the highly fluctuating nature of the RCS pattern. The term complex refers to the type of scattering expected from a target consisting of many scattering centers. In addition, due to the dynamic nature of the aircraft/radar engagement it is not possible to completely characterize the RCS deterministically for every possible observation

angle. A complete characterization of the RCS would require both the azimuth and elevation RCS data in very small increments, i.e. on the order of tenths of a degree for typical targets. Even if we did measure the RCS at all angles of interest, it would not be feasible to handle this huge amount of data, and the data would most likely be reduced or compressed via statistical processing techniques.

Given that a deterministic method for characterizing the RCS is not feasible for the complex target, a statistical approach is considered. The key ingredients in a statistical characterization is the RCS probability density function and the second order moment of the RCS. The second order moment describes how the RCS is expected to fluctuate from a particular observation angle to another observation angle. If we are interested in characterizing how the RCS fluctuations affect the probability of detection, then we need to know how the second order moment of the RCS affects the pulse-to-pulse correlation of the received return signal and how this pulse-to-pulse correlation affects the probability of detection. The purpose of this thesis is to investigate how the RCS fluctuations affect the pulse-to-pulse correlation of the received signal. With this purpose in mind, two questions naturally arise. The first is how important is the pulse-to-pulse correlation of the reflected radar signal in determining the detection of the target? The second question is if the pulse-to-pulse correlation is important, how do we determine the correlation properties for a given target? The first question can be answered by quantifying how the pulse-to-pulse correlation properties of the RCS affect target detectability. The second question can be answered by developing analytic models which describe the target fluctuations. Unfortunately, there has only been a limited amount of work performed on the correlated nature of radar return signals. Thus, before we can answer the angular sampling question, we must develop a partially correlated radar detection model and determine a method for predicting the signal correlation parameters.

1.2 Goals

The primary goal of this thesis is to investigate the importance of the pulse-to-pulse correlation of the radar returns on the probability of detection (P_D). The second goal is to determine a method for predicting the pulse-to-pulse correlation characteristic without explicitly making the required detailed measurements.

1.3 Approach

In order to understand how the pulse-to-pulse correlation affects the target detectability, a detection model is developed that explicitly incorporates the effects of pulse-to-pulse correlation. Chapter 2 introduces the radar receiver system used to investigate the detection of partially correlated return signals. The radar receiver model consists of a quadrature demodulator receiver, followed by a square law envelope detector and a linear post-detection integrator. The Neyman-Pearson detection criteria is used to determine the probability of detection. Using the Neyman-Pearson criteria, four techniques for calculating the probability of detection of a target by a pulsed search radar are introduced. I will then use these techniques to investigate the importance of the pulse-to-pulse correlation of the received signal in determining P_D of the target.

Once the importance of the pulse-to-pulse correlation on P_D is shown, it is necessary to establish a method for predicting this correlation characteristic. Chapter 3 develops the analytic models to predict this pulse-to-pulse correlation. After the analytic correlation models are developed, it will be possible to determine the target detectability using the detection techniques of chapter 2. Using the results from the general correlation models, we will generate the target autocorrelation function of two different distributions of the RCS scattering centers. The final section of this chapter gives an empirical approach for estimating the pulse-to-pulse correlation using measured RCS data.

Having an understanding of the importance of the affects of the pulse-to-pulse correlation properties in chapter 3, I seek to develop a method to actually predict these properties for a complex target. Chapter 4 illustrates how these properties can be predicted for an AIM-9 missile. Finally, chapter 5 illustrates how the correlation models and the radar detection technique of chapter 2 are used to determine the probability of detection for a given radar/aircraft engagement.

II. Radar Detection Calculations

Developing a radar detection model is the first step required to investigate how the target RCS fluctuations affect the detectability of a target. Pulsed radar systems typically integrate tens to hundreds of pulses to improve the detection probability. The process of summing all the radar return pulses for the purpose of improving detection is called integration (17). For the pulsed radar system integrators we want to know the importance of the pulse-to-pulse correlation in calculating P_D.

This chapter introduces the radar receiver system and the Neyman-Pearson detection criteria used to determine the probability of detection. Four techniques for calculating the probability of detection by a pulsed search radar are then introduced. The first technique is based on the early work of Peter Swerling (19). While this technique does not incorporate the pulse-to-pulse correlation properties of the radar return, it is included since it has become a virtual "standard" for calculating radar detection ranges for high frequency radar systems. The Swerling results are also useful as a baseline to compare with the other calculations. The second detection calculation technique is also developed by Swerling (18). The pulse-to-pulse correlation is modeled in the received signal covariance matrix and P_D is determined by the eigenvalues of this matrix. The signal covariance matrix and eigenvalues are describe in section 2.3. Next, Irving Kanter's (14) technique for determining the eigenvalues of the signal covariance matrix is introduced. Unfortunately, summation errors associated with this technique limit the number of integrated pulses to less than 30. The final detection technique, by Carl Helstrom (12), solves the summation error problem through the use of contour and saddlepoint integration techniques.

2.1 Pulsed Radar Receiver Model

The radar receiver model consists of a quadrature demodulator receiver, followed by a square law envelope detector and a linear post-detection integrator. A

block diagram of the receiver structure is given in Fig 2.1. This receiver represents the optimum detection receiver structure for small signal-to-noise ratio signals (5).
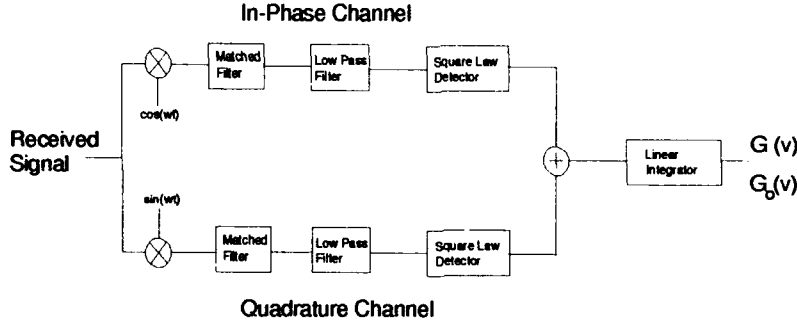
Figure 2.1. Radar Receiver Block Diagram

The radar receiver noise is assumed to be additive, zero mean Gaussian. We will also assume that the envelope of each pulse out of the square law detector is sampled at a time when the received signal is expected to peak in the absence of noise. This sampling is then repeated for each of the N received pulses. Let the detector output for each pulse be normalized by the receiver noise power, $2\beta^2$. The normalized output from the integrators for N pulses is

$$v = \frac{1}{2\beta^2} \sum_{i=1}^{N} z_i, \qquad z_i = \mid x_i + jy_i \mid^2 \tag{2.1}$$

where x_i and y_i are the in-phase and quadrature phase signals of the ith pulse through the square law detectors.

The following notation will be used to defined the various quantities used in this chapter. Hypothesis H_1 is used to represent the condition when the received signal consists of the target return plus noise, and hypothesis H_o represents the condition where noise alone is present. $G(v)$ is used to represent the integrator output probability density function (pdf) of the N received signals for the H_1 hypothesis, and $G_o(v)$ represents the output for the H_o hypothesis. Figure 2.2 illustrates a

representative example of the integrator output pdf's $G(v)$ and $G_o(v)$. Additionally,
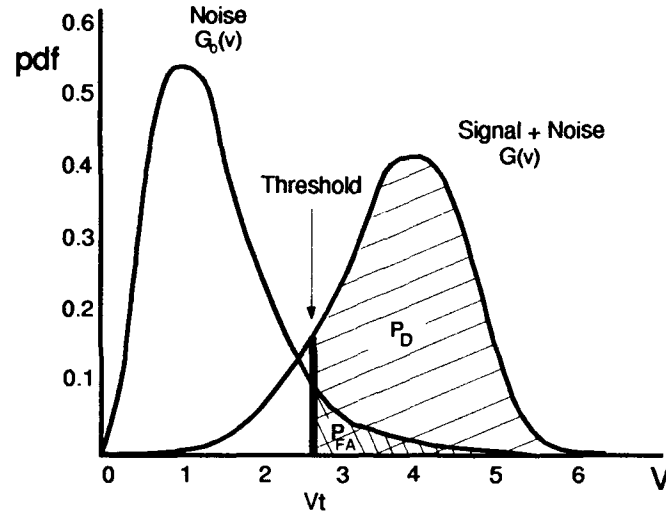
Figure 2.2. Detector Output pdf

we will define the per pulse ratio of signal power to average noise power by

$$\chi \doteq \frac{\bar{z}}{2\beta^2},$$ (2.2)

where $\bar{z}$ is the mean value of the received signal through the detectors.

2.1.1 Neyman-Pearson Detection Criteria The Neyman-Pearson detection criteria, which is most often used in radar, maximizes the detection probability for a fixed probability of false alarm, P_{FA}. Using the Neyman-Pearson criteria, the detection threshold, (V_T) is determined by the pdf of the noise only signal, $G_o(v)$, and the desired P_{FA}. The P_{FA} is calculated by integrating $G_o(v)$ from V_T to infinity. Once the threshold has been determined, the probability of detection is calculated by integrating the signal plus noise conditional pdf, $G(v)$ from V_T to infinity. These quantities are explicitly given by:

$$P_{FA} = \int_{V_t}^{\infty} G_o(v)dv$$ (2.3)

$$P_D = \int_{V_t}^{\infty} G(v) dv \tag{2.4}$$

Solving for the threshold level, V_T, is relatively easy if the system noise has a Gaussian distribution. For this case P_{FA} can easily be written as (14)

$$P_{FA} = e^{-V_t} \sum_{n=0}^{N-1} \frac{V_T^n}{n!}. \tag{2.5}$$

Determining the P_D is difficult, since the pdf of the integrator output statistic, $G(v)$, depends on the fluctuating radar return signal and the pulse-to-pulse correlation properties. These fluctuations and the pulse-to-pulse correlation properties in turn depend on the target's RCS, the movement of the aircraft or radar within the N pulse integration period, and the radar's pulse repetition frequency (prf). The first attempt at calculating the P_D is to simply assume a form for $G(v)$, and model the individual return pulses as being either completely correlated or completely uncorrelated. This assumption greatly simplifies the mathematics involved and allows us to calculate P_D in an easy manner.

2.2 Swerling Fluctuation Models

The first technique we will consider for calculating the P_D was developed by Peter Swerling (19). The resulting models developed using this technique are the most commonly used to predict the target detection probability. Swerling (19) uses two target model pdf's $p(z)$ to describe the pulse signal fluctuations through the square law detector. These two fluctuation models describe the signal amplitude fluctuations and have been found to correspond to many types of targets. The first pdf studied by Swerling is expressed by the Rayleigh distribution (negative-exponential),

$$p(z) = \frac{1}{\bar{z}} \exp\left(-\frac{z}{\bar{z}}\right), \qquad z \geq 0 \quad , \tag{2.6}$$

where z is the input signal power and $\bar{z}$ is the average signal power. The second target pdf studied by Swerling is given as a chi-square distribution,

$$p(z) = \frac{4z}{\bar{z}^2} \exp\left(-\frac{2z}{\bar{z}}\right), \qquad z \geq 0. \tag{2.7}$$

In addition to the two target pdf's, Swerling assumes two types of signal fluctuations from one pulse to the next pulse. In the first case, the signal amplitude is assumed to be completely correlated for each pulse within a single scan of the radar. For the second case, the pulses are assumed to be un-correlated from pulse-to-pulse. The two target fluctuation pdf's and the two pulse-to-pulse fluctuation models are combined to yield the four well known Swerling fluctuation models used in detectability studies. The four models are shown in Table 2.1.

Table 2.1. Swerling Fluctuation Models

Target pdf	Scan-to-Scan Signal Fluctuations	Pulse-to-Pulse Signal Fluctuations
$p(z) = \frac{1}{\bar{z}} \exp\left(-\frac{z}{\bar{z}}\right)$	SW1	SW2
$p(z) = \frac{4z}{\bar{z}^2} \exp\left(-\frac{2z}{\bar{z}}\right)$	SW3	SW4

2.2.1 Swerling Models Deciding which Swerling model to use in a detectability study depends on the target's RCS scintillation characteristics, and on the pulse repetition frequency (prf) of the radar. If the target can be represented as a collection of many independently fluctuating reflectors of approximately equal magnitude, then the pdf of the detector output is close to the Rayleigh pdf given in eqn 2.6. Experimentally it has been shown that if the number of reflectors is as small as four or five the pdf can still be approximated by this pdf. Targets which can be represented

as one large reflector with a number of smaller reflectors are more appropriately modeled with the pdf in eqn 2.7 (8).

The choice of scan-to-scan or pulse-to-pulse fluctuations is determined by the radar's prf and the RCS characteristics of the target. The scan-to-scan model applies to jet aircraft or missiles where the phase scattering centers may be moving slowly compared to the radar's prf. Pulse-to-pulse fluctuations would apply to propeller-driven aircraft if the propellers contribute a large portion of the echoing area, or if the engine components are within the radar's line-of-sight. Targets for which very small changes in orientation would mean large changes in cross section, or targets viewed by a radar with sufficiently low pulse repetition rates would also be modeled with a pulse-to-pulse signal fluctuation model (8).

In the later investigation of the effects of partial pulse-to-pulse correlation we are restricted to Rayleigh distributions for the square law detector output z. Therefore, we will only concentrate on the $SW1$ and $SW2$ detection models. A simple form for P_D for N un-correlated return signals, $SW2$, is given by Irving Kanter (14) as:

$$P_D = \exp\left(-\frac{V_T}{1+\chi}\right) \sum_{n=0}^{N-1} \left[\frac{V_T}{1+\chi}\right]^n \frac{1}{n!} \qquad (2.8)$$

Similarly, for completely correlated return signals, $SW1$, P_D is given by:

$$P_D = P_{FA} + \frac{e^{-V_T}}{1+N\chi} \sum_{n=1}^{\infty} \left(\frac{N\chi}{1+N\chi}\right)^n \sum_{k=N}^{N-1+n} \frac{V_T^k}{k!} \qquad (2.9)$$

The Swerling models are virtually a "standard" for radar detection-range calculations (2) and provide a baseline to compare to the partially correlated detection models. Difranco and Rubin (5) provide a good description on the use and selection of the proper Swerling models for detectability studies.

2.3 Partially Correlated Radar Pulses

The Swerling models are important since they are the most widely used models in radar detection studies; however, these four models consider only the cases where the signal is either completely correlated ($SW1$ and $SW3$) or completely uncorrelated ($SW2$ and $SW4$) from pulse-to-pulse. Continuing his early development, Swerling (18) extended his detection theory to the more general case of partially correlated radar return pulses. Recall that the probability of detection, P_D, and probability false alarm, P_{FA}, are given by

$$P_{FA} = \int_{V_t}^{\infty} G_o(v)dv = e^{-V_t} \sum_{n=0}^{N-1} \frac{V_T^n}{n!}$$

$$P_D = \int_{V_t}^{\infty} G(v)dv,$$

and

$$v = \frac{1}{2\beta^2} \sum_{i=1}^{N} z_i, \qquad z_i = |x_i + jy_i|^2,$$

where x_i and y_i are the in-phase and quadrature phase of the received signal and N is the number of integrated pulses. These components are assumed to be Gaussian random variables with zero mean. In addition, z_i is assumed to be statistically independent of the receiver noise. For the signal plus noise case, hypothesis H_1, calculation of P_D is difficult, since the statistics of v depends on the fluctuating radar return signal and on the pulse-to-pulse correlation properties. These fluctuations and pulse-to-pulse correlation properties in turn depend on the radar's prf and the movement of the aircraft or radar within the N pulse integration period.

To calculate P_D, we begin by manipulating $G(v)$ into a form which can be easily integrated by taking the Laplace transform of $G(v)$ and simplifying the resulting equation. P_D can then be determined by taking the inverse Laplace transform of

this result and integrating $G(v)$ from V_T to infinity. Since the steps involved in simplifying the Laplace transform of $G(v)$ are numerous, only the results will be given here. The complete derivation which closely follows Swerling's paper (18) is given in Appendix A.

The Laplace transform, $L(s)$, of $G(v)$ is given as

$$L(s) = \int_0^\infty e^{-sv} G(v) dv. \tag{2.10}$$

After much manipulation, the simplified expression for the Laplace transform of $G(v)$ is given as

$$L(s) = \prod_{i=1}^N \frac{1}{1 + s(1 + \lambda_i)}, \tag{2.11}$$

where λ_i is the ith eigenvalue of the signal covariance matrix C. The individual elements of the signal covariance matrix are given as

$$c_{i,j} = E[z_i z_j], \qquad i = 1 \cdots N, \qquad j = 1 \cdots N, \tag{2.12}$$

where $E[]$ is the expectation operator. As stated earlier, the pulse-to-pulse correlation is primarily due changes in the target RCS within the N pulse integration period. All of the pulse-to-pulse correlation information is contained by eqn 2.12 and the resulting covariance matrix, C.

P_D is then determined by taking the inverse Laplace transform of eqn 2.11 and integrating the resultant pdf from V_T to infinity. The inverse Laplace transform of eqn 2.11 gives the following simplified form for $G(v)$:

$$G(v) = \sum_{n=1}^N \prod_{\substack{k=1 \\ k \neq n}}^N \left[\left(1 - \frac{1 + \lambda_k}{1 + \lambda_n} \right) \right]^{-1} \frac{\exp[\frac{-v}{1+\lambda_n}]}{1 + \lambda_n} \tag{2.13}$$

Integrating this pdf from V_T to infinity yields P_D, which after simplification can be written as:

$$P_D = \sum_{n=1}^{N} \prod_{\substack{k=1 \\ k \neq n}}^{N} \left[\left(1 - \frac{1 + \chi\lambda_k}{1 + \chi\lambda_n} \right) \right]^{-1} \exp\left(\frac{-V_T}{1 + \chi\lambda_n} \right). \qquad (2.14)$$

Equation 2.14 gives the desired P_D for a Rayleigh distributed signal, assuming the eigenvalues of the signal covariance matrix are known. While this technique is relatively straight forward, it is difficult to use because of the need to determine the N eigenvalues of a N by N signal covariance matrix. The difficulty of computing the covariance matrix eigenvalues can be overcome by a technique developed by Irving Kanter (14) discussed in the next section.

2.4 Signal Covariance Matrix and Eigenvalues

The third technique for calculating the probability of detection of Rayleigh distributed radar returns is given by Irving Kanter (14). Kanter also addresses how to calculate the inverse Laplace transform of $L(s)$, and how to determine the eigenvalues of the covariance matrix. An alternative technique for calculating $L(s)$ is used, but the same results as determined by Swerling in eqn 2.11 are obtained. The technique of computing the signal covariance matrix eigenvalues introduced by Kanter allows us to easily determine P_D.

This section closely follows the work of Kanter (14) and shows how the covariance matrix eigenvalues are determined. We begin by first considering the nature of the received signal covariance matrix. If the received radar pulses arise from a stationary process, then the signal covariance matrix, C, will be a symmetric Toeplitz matrix with N distinct elements (14). With this observation in mind, we will assume that the received signal may be described by a first order Markov process. The justification for this assumption is based on target fluctuation characteristics observed by Barton (1), and on flight test measurements conducted by Edrington(7) which showed the detector output to be exponentially correlated for three different types

2-9

of aircraft. Using this assumption, P_D is determined from the eigenvalues of the signal covariance matrix which is characterized by a single correlation parameter ρ. Using these observations, the c_{kn} element of the covariance matrix, for a train of N uniformly spaced pulses, is given by

$$c_{kn} \doteq \rho^{|k-n|} \qquad 0 \leq \rho \leq 1, \qquad (2.15)$$

and the resulting signal covariance matrix is

$$C = \begin{bmatrix} 1 & \rho & \cdots & \rho^{N-1} \\ \rho & 1 & \rho & \vdots \\ \vdots & \ddots & \ddots & \rho \\ \rho^{N-1} & \cdots & \rho & 1 \end{bmatrix} \qquad (2.16)$$

The eigenvalues of C provide a nontrivial solution to the matrix equation

$$[C - \lambda I]\, U = 0 \qquad (2.17)$$

where I is an N by N identity matrix and U is a N dimensional vector with individual elements $u_o, \cdots, u_{N-1}$. In addition, the sum of the eigenvalues equals the trace of C giving the relation

$$\sum_{i=1}^{N} \lambda_n = N, \qquad (2.18)$$

which will be used later on.

As an example, consider the special case where the interpulse spacing is so large that the correlation of non-consecutive pulses may be neglected. For this case, the signal covariance matrix is tridiagonal and eqn 2.17 is equivalent to a homogeneous boundary value problem (14), which can be expressed as a set of homogeneous second

order difference equations of the form

$$\rho u_{n-1} + (1 - \lambda)u_n + \rho u_{n+1} = 0, \qquad n = 1, \cdots, N \ , \qquad (2.19)$$

with the homogeneous boundary conditions,

$$u_o = u_{N+1} = 0. \qquad (2.20)$$

Since eqn 2.19 is linear and has constant coefficients, there are two solutions of the form

$$u_n = \gamma^n, \qquad (2.21)$$

where

$$\gamma = \frac{\lambda - 1}{2\rho} \pm \sqrt{\left(\frac{\lambda - 1}{2\rho}\right)^2 - 1}. \qquad (2.22)$$

The condition $\mid (\lambda - 1)/2\rho \mid \geq 1$ implies either $\lambda \geq 1 + 2\rho$ or $\lambda \leq 1 - 2\rho$, each of which leads to a contradiction of eqn 2.18. Thus, we must have $\mid (\lambda - 1)/2\rho \mid < 1$, and γ can be expressed as $\gamma = e^{\pm j\theta}$. Using the identity, $e^{\pm j\theta} = \cos\theta \pm j\sin\theta$, the real part of eqn 2.22 can then be expressed as:

$$\cos\theta \doteq \frac{\lambda - 1}{2\rho} \qquad (2.23)$$

The general solution to eqn 2.19 in terms of $e^{\pm jn\theta}$ can be written as

$$u_n = K_1 \cos n\theta + K_2 \sin n\theta \qquad (2.24)$$

Since the boundary condition $u_0 = 0$ must be satisfied, K_1 must equal zero. The second boundary, $u_{N+1} = 0$, allows us to solve the transcendental equation 2.24 for θ. Rewriting eqn 2.24 for $n = N + 1$ gives

$$u_{N+1} = K_2 \sin(N + 1)\theta = 0. \qquad (2.25)$$

Equation 2.25 then yields the distinct θ_n values:

$$\theta_n = \frac{n}{N+1}\pi, \qquad n = 1, \cdots, N \qquad (2.26)$$

Note that the θ_n's are equally spaced in the open interval $(0, \pi)$. Equation 2.23 yields the N signal covariance matrix eigenvalues

$$1 - 2\rho < \lambda_n = 1 + 2\rho\cos\theta_n < 1 + 2\rho, \qquad n = 1, \cdots, N. \qquad (2.27)$$

The following example of solving for the probability of detection using this technique, will help to clarify the steps involved. Consider the case of two integrated pulses. The covariance matrix is given as

$$C = \begin{bmatrix} 1 & \rho \\ \rho & 1 \end{bmatrix} \qquad (2.28)$$

From eqn 2.26, $\theta_1 = \pi/3$ and $\theta_2 = 2\pi/3$. The eigenvalues are determined from eqn 2.27 and are given as

$$\lambda = 1 \pm \rho. \qquad (2.29)$$

The probability of detection, P_D, from our earlier results eqn 2.14, is given as

$$P_D = \sum_{n=1}^{2} \prod_{\substack{k=1 \\ k \neq n}}^{2} \left[1 - \frac{1 - \chi\lambda_k}{1 + \chi\lambda_n}\right]^{-1} \exp\left(-\frac{V_t}{1 + \chi\lambda_n}\right), \qquad (2.30)$$

where V_T is the signal threshold required for a given P_{FA} and χ is the per pulse ratio of signal power to average noise power, and $\lambda_{1,2} = 1 \pm \rho$. Substituting in the eigenvalues and simplifying, results in the P_D given by

$$P_D = \exp\left\{\frac{-(1+\chi)V_T}{(1+\chi)^2 - (\rho\chi)^2}\right\} * \left[\frac{1+\chi}{\rho\chi}\sinh\left(\frac{\rho\chi V_T}{(1+\chi)^2 - (\rho\chi)^2}\right) + \cosh\left(\frac{\rho\chi V_T}{(1+\chi)^2 - (\rho\chi)^2}\right)\right]$$

This result agrees with the value calculated by Schwartz (16) for two integrated pulses. For the case where the correlation of non-consecutive pulses may not be ignored, a similar technique of formulating and solving an equivalent homogeneous boundary value problem may be applied. Since this is the case more frequently encountered, the derivation given in Kanter's paper (14) is included in Appendix B.

Evaluating the P_D by this technique is difficult when $N > 30$, since the first terms in the series of eqn 2.14 are large when the eigenvalues are close together in magnitude, which will be the case when N is large. As shown in section 2.6.5, the summation errors associated with this technique become too large, and an alternative technique for determining P_D is required.

2.5 Calculating P_D Using Contour Integration

The final technique for determining the P_D of Rayleigh distributed signals is based on the work of Carl Helstrom (12). The difficulty of the summation errors of Kanter's technique can be avoided through the use of saddle-point integration and it's associated saddlepoint approximations. The use of contour integration to determine P_D is also introduced in this section. The contour integration technique gives the same results for P_D given earlier; however, the notation is slightly different.

Before we introduce the saddlepoint integration techniques, we will first show how P_D can also be determined by contour integration. Recall from our earlier results that the Laplace transform of the detector output is given by

$$L(s) = \prod_{i=1}^{N} \frac{1}{1 + s(1 + \lambda_i)} \tag{2.31}$$

Equation 2.31 and the resultant derivation can be simplified by defining α_k as:

$$\alpha_k \doteq 1 + \lambda_k \tag{2.32}$$

Rewriting the Laplace transform of $G(v)$, eqn 2.31, in terms of α gives:

$$L(s) = \prod_{i=1}^{N} \frac{1}{1 + \alpha_k s} \qquad (2.33)$$

As shown earlier, P_D is given as the integral of $G(v)$ from the threshold to infinity. In the two previous techniques, $G(v)$ was determined from the inverse Laplace transform of $L(s)$. P_D was then determined by integration of $G(v)$ over the appropriate limits. An alternative technique for calculating P_D is to transform the integration limits to the s-plane and perform the appropriate contour integration. This is the technique used by Helstrom (12). To use this technique, we begin with the moment-generating function, $h(s)$, of the statistic v. The moment-generating function is given by:

$$h(s) = E[e^{-sv}] = [D(s)]^{-1}, \qquad (2.34)$$

where

$$D(s) = \prod_{k=1}^{N} (1 + \alpha_k s). \qquad (2.35)$$

The cumulative distribution function, cdf, is the integral of $G(v)$ from 0 to V_T, which is equal to $1 - P_D$. The cdf is generated from the moment generating function $h(s)$ by the inverse Laplace transform of eqn 2.33 and is given by

$$q_-(V_T) = 1 - P_D = \int_{c-j\infty}^{c+j\infty} (s)^{-1} h(s) e^{sV_T} \frac{ds}{j2\pi}, \qquad c > 0, \qquad (2.36)$$

with integration along a straight vertical contour in the right half-plane. The complementary cumulative distribution function, ccdf, and the P_D are given as the integral of $G(v)$ from V_T to infinity. The ccdf is given by

$$q_+(V_T) = P_D = \int_{c-j\infty}^{c+j\infty} (-s)^{-1} h(s) e^{sV_T} \frac{ds}{j2\pi}, \qquad c < 0. \qquad (2.37)$$

2-14

with integration in the portion of the converging strip of the Laplace transform $h(s)$ in the left half-plane. The N poles of $h(s)$ lie at the points $s_k = \frac{-1}{\alpha_k}$, and $c > \frac{-1}{\alpha_1}$, where α_1 is the largest of the scaled eigenvalues of the C matrix. The residue theorem is then used to evaluate the P_D (10). The resultant P_D is given by

$$P_D = q_+(V_T) = \sum_{k=1}^{N} \prod_{\substack{n=1 \\ n \neq k}}^{N} \left[1 - \frac{\alpha_n}{\alpha_k} \right]^{-1} \exp\left(\frac{-V_T}{\alpha_k} \right). \qquad (2.38)$$

This technique of determining the P_D gives the same results developed by Kanter (14) and Swerling (18), and it has the same limitations they encountered. Recall, the first terms in the series are large when the signal covariance matrix eigenvalues are of approximately the same magnitude. The ill behavior of the summation errors in eqn 2.38 can be avoided by evaluating eqn's 2.36 and 2.37 using saddlepoint integration and the corresponding saddlepoint approximations introduced by Helstrom (10).

2.5.1 Saddlepoint Integration of $q_\pm(V_T)$ The saddlepoint integration technique is described in detail in references (9),(10), and (11). The general approach to this technique starts with the integrals of the type described in eqn's 2.36 and 2.37 which have the form

$$q_\pm(V_T) = \int_{c-j\infty}^{c+j\infty} e^{\Phi(s)} \frac{ds}{j2\pi}, \qquad (2.39)$$

where the "phase" term $\Phi(s)$ is given by the moment-generating function, eqn's 2.34 and 2.35, which when simplified results in

$$\Phi(s) = V_T s - \sum_{k=1}^{N} \ln(1 + \alpha_k s) - \ln(\mp s). \qquad (2.40)$$

P_D is computed by deforming the contour of integration onto a path passing through the saddlepoint s_o^- or s_o^+ of the integrand of eqn 2.39 on the Re s−axis. The saddle-

points are roots of the equation

$$\Phi'(s) = V_T - \sum_{k=1}^{N} \alpha_k(1 + \alpha_k s)^{-1} - s^{-1} = 0, \tag{2.41}$$

$$s = s_o^-, s_o^+, \quad -\alpha_1^{-1} < s_o^- < 0, \quad s_o^+ > 0.$$

The roots of eqn 2.41 are computed using Newton's method where each trial value of s' is replaced by

$$s' \leftarrow s' - \frac{\Phi'(s')}{\Phi''(s')} \tag{2.42}$$

with

$$\Phi''(s) = \sum_{k=1}^{N} \alpha_k^2(1 + \alpha_k s)^{-2} + s^{-2}. \tag{2.43}$$

The above procedure determines the saddlepoint s_o^+ or s_o^-. The cdf and ccdf are determined by the saddlepoint approximation:

$$q_{\pm}(V_T) \approx [2\pi\Phi''(s_o^{\mp})]^{-\frac{1}{2}} \exp(\Phi(s_o^{\mp})) \tag{2.44}$$

The probability of detection can be determined from either the cdf or the ccdf, and is given as

$$P_D = q_+(V_T) \approx [2\pi\Phi''(s_o^-)]^{-\frac{1}{2}} \exp(\Phi(s_o^-)). \tag{2.45}$$

$$P_D = 1 - q_-(V_T) \approx 1 - [2\pi\Phi''(s_o^+)]^{-\frac{1}{2}} \exp(\Phi(s_o^+)). \tag{2.46}$$

When $N \gg 1$ these approximations are adequate.

Now that we have a technique to determine P_D for correlated Rayleigh return signals, the next step is to use these models to show how P_D is determined for different covariance matrixes. In-addition, the next section will also show the summation error problem encountered by Irving Kanter.

2.6 Detection Calculations

This section discusses the actual calculation of P_D using the Kanter and Helstrom techniques described earlier. The detection calculation technique of Kanter (14) was implemented first. This method yields acceptable results for up to $N = 30$ pulses, and for correlation coefficients $\rho \leq 0.9$. For larger number of pulses and for higher correlation coefficients, the summation errors are too large. The technique of Helstrom (12) was implemented next to overcome this limitation. This technique yields acceptable results for all cases considered. For each technique the algorithms were written in FORTRAN 77 source code. The steps involved for calculating the probability of detection are:

Determine the detection threshold, V_T.

Calculate the covariance matrix, C, for N pulses.

Calculate the C matrix eigenvalues, λ_i.

Determine the probability of detection using eqn 2.14 or 2.45.

2.6.1 Detection Threshold V_T

Recall, the detection threshold, V_T, is the required noise signal threshold to a achieve a given P_{FA}. Unless otherwise specified this P_{FA} was set to 10^{-6}. Since the threshold is independent of the target signal, the threshold values are calculated in advance and stored in a data file. The following technique provides an effective way of calculating the threshold. An initial estimate of the threshold is given by (6),

$$V_T \approx \sqrt{N}\Phi^{-1}(P_{FA}) + N, \qquad (2.47)$$

where $\Phi^{-1}(P_{FA})$ is a constant found on page 368 of Difranco and Rubin (6). This approximation is valid for $10^{-2} \leq P_{FA} \leq 10^{-15}$ (6). A more accurate threshold is then calculated using our earlier results for P_{FA}

$$P_{FA} = e^{-V_T} \sum_{n=0}^{N-1} \frac{V_T}{n!}, \qquad (2.48)$$

where V_T is varied and the calculated P_{FA} is compared to the desired value. When the difference is within an allowable limit, the threshold value, V_T, is written to the appropriate data file.

2.6.2 Covariance Matrix C With the appropriate value of V_T calculated for N pulses, the next step is calculate the covariance matrix. For the initial evaluation of this technique, an exponential correlation model described by Kanter (14) was used. For this case the received signal consists of a train of N pulses with uniform spacing between the individual pulses. The c_{kn} value of the covariance matrix are given as

$$c_{kn} \doteq \rho^{|k-n|}, \qquad (2.49)$$

$$C = \begin{bmatrix} 1 & \rho & \rho^2 & \cdots & \rho^{N-1} \\ \rho & 1 & \rho & \cdots & \rho^{N-2} \\ \vdots & \ddots & \ddots & \ddots & \vdots \\ \rho^{N-2} & \cdots & \rho & 1 & \rho \\ \rho^{N-1} & \cdots & \rho^2 & \rho & 1 \end{bmatrix}. \qquad (2.50)$$

2.6.3 Determination of C Eigenvalues λ_i The eigenvalues of the C matrix were determined using the IMSL DEVCSF FORTRAN subroutine (13). This subroutine determines the double precision eigenvalues for a real symmetric matrix using the method mentioned below.

> Routine DEVCSF computes the eigenvalues and eigenvectors of a real symmetric matrix as follows: first, accumulating orthogonal similarity transformations are used to reduce the matrix to an equivalent symmetric tridiagonal matrix; second, the implicit QL algorithm is used to compute the eigenvalues and eigenvectors of this tridiagonal matrix. The

eigenvectors are normalized such that the ∞-norm of each eigenvector is one (13).

The calculated eigenvalues were then compared to the eigenvalues calculated using Kanter's (14) technique. For the cases considered, the two techniques produced the same results.

2.6.4   Calculation of P_D   The last step is to determine the P_D curves for various signal-to-noise ratios. Recall our earlier results for P_D was given as

$$P_D = \sum_{n=1}^{N} \prod_{\substack{k=1 \\ k \neq n}}^{N} \left[1 - \frac{1 - \chi\lambda_k}{1 + \chi\lambda_n} \right]^{-1} \exp\left[\frac{-V_t}{1 + \chi\lambda_n} \right], \tag{2.51}$$

where χ is the signal-to-noise ratio.

2.6.5   Kanter Results   The above technique yields results which agree with the values calculated by Kanter (14). Unfortunately, as ρ approaches 1. or for $N \geq 30$ the summation errors become too large and the results become unacceptable for small signal-to-noise ratios. An illustration of these results are shown in Fig 2.3.

For $\rho = 0.8$ and $\rho = 0.9$, the summation error is too large. The magnitude of this error increases as the number of integrated pulses increases and/or as the correlation coefficient, ρ increases. Since this technique limits the number of pulses to be less than 30, this technique was abandoned for the Helstrom saddlepoint integration technique described in the next section.

2.6.6   Saddlepoint Integration Method   The Helstrom technique is similar to the Kanter technique. The major difference is that saddlepoint integration techniques are utilized to perform the calculation of P_D (12). This integration technique avoids summation errors encountered with the Kanter technique. The algorithm developed in the previous section was used to determine the detection threshold V_T. The covariance matrix eigenvalues were also calculated by the technique described in
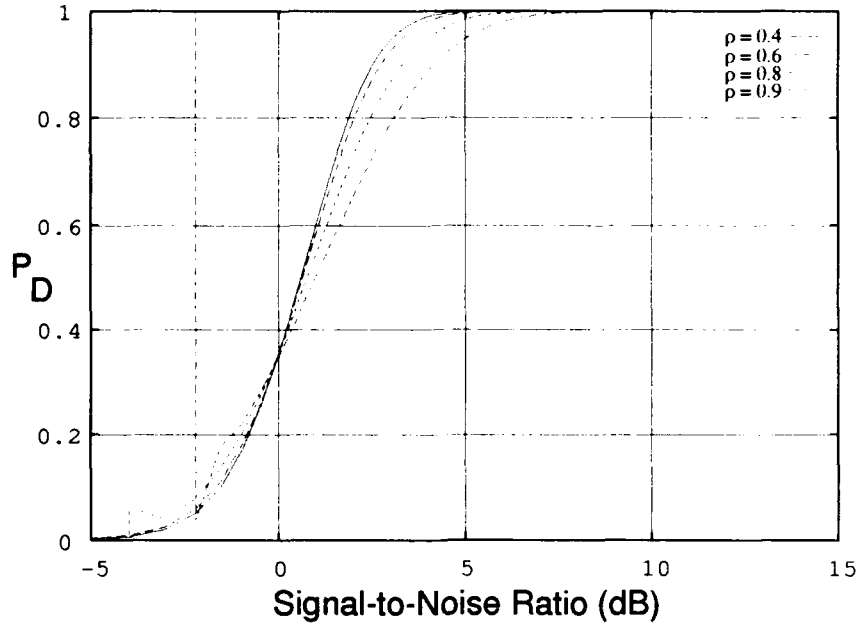
Figure 2.3. Kanter's Method for $N = 30$ pulses integrated

the previous section. A detailed discussion of the saddlepoint integration technique is given in chapter 2.

Recall the saddlepoints are roots of eqn 2.52 and are used to determine P_D.

$$\Phi'(s) = V_T - \sum_{k=1}^{N} \alpha_k (1 + \alpha_k s)^{-1} - s^{-1} = 0, \tag{2.52}$$

$$s = s_o^-, s_o^+, \qquad -\alpha_k^{-1} < s_o^- < 0, \qquad s_o^+ > 0$$

The saddlepoints are computed by Newton's method where each trial value of s' is replaced by

$$s' \leftarrow s' - \frac{\Phi'(s')}{\Phi''(s')} \tag{2.53}$$

with

$$\Phi''(s) = \sum_{k=1}^{N} \alpha_k^2 (1 + \alpha_k)^{-2} + s^{-2}. \tag{2.51}$$

2-20

The above procedure determines the saddlepoint. The cdf and ccdf are determined using the saddlepoint approximation

$$q_{\pm}(V_T) \approx [2\pi\Phi''(s_o^{\mp})]^{.5}\exp(\Phi(s_o^{\mp})). \tag{2.55}$$

The probability of detection can be determined from either the cdf or the ccdf by:

$$P_D = q_+(V_T) \approx [2\pi\Phi''(s_o^{-})]^{.5}\exp(\Phi(s_o^{-})). \tag{2.56}$$

$$P_D = 1 - q_-(V_T) \approx 1 - [2\pi\Phi''(s_o^{+})]^{.5}\exp(\Phi(s_o^{+})). \tag{2.57}$$

A plot of P_D using this technique for 30 pulses is shown in figure 2.4. As the figures demonstrate, the summation error associated with the earlier technique is avoided. Figure 2.5 shows the P_D curve for 150 pulses integrated. Again there are no noticeable anomalies associated with this technique even for highly correlated pulses.

Some observations about the results shown in Fig's 2.4 and 2.5 are useful. Smaller values of ρ correspond to signals which are less correlated, i.e. more fluctuating from pulse-to-pulse. For $P_D < 0.4$ the degree of correlation makes little difference, the more fluctuating signals are almost identical to the less fluctuating signals. Note that the $\rho = 0.4$ is close to the $\rho = 0.6$ curve, while the $\rho = 0.9$ is more spread out than $\rho = 0.95$. Having the curves that correspond to the higher fluctuating targets to the left of the less fluctuating curves implies the fluctuating targets require a lower signal-to-noise ratio to achieve a given P_D. Figure 2.4 shows the importance of the correlation properties in determining P_D. For a P_D of 0.95, the $\rho = 0.95$ correlation coefficient requires an additional signal-to-noise of 1.7 dB to achieve the same P_D as the $\rho = 0.4$ correlation coefficient.

The preceding analysis calculates P_D using an exponential correlation parameter. Recall that the exponential correlation parameter allows us to compute the
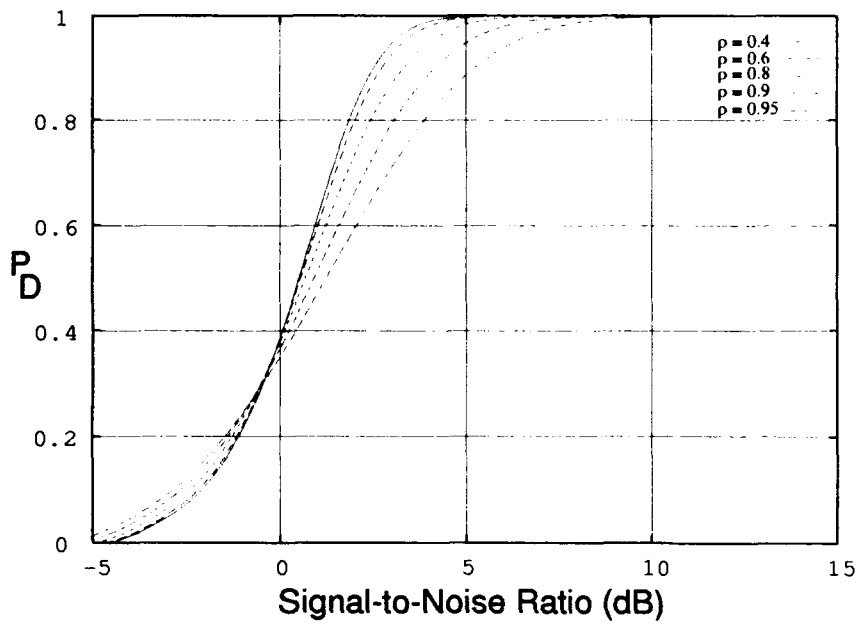
Figure 2.4. Saddlepoint Integration for 30 radar pulses
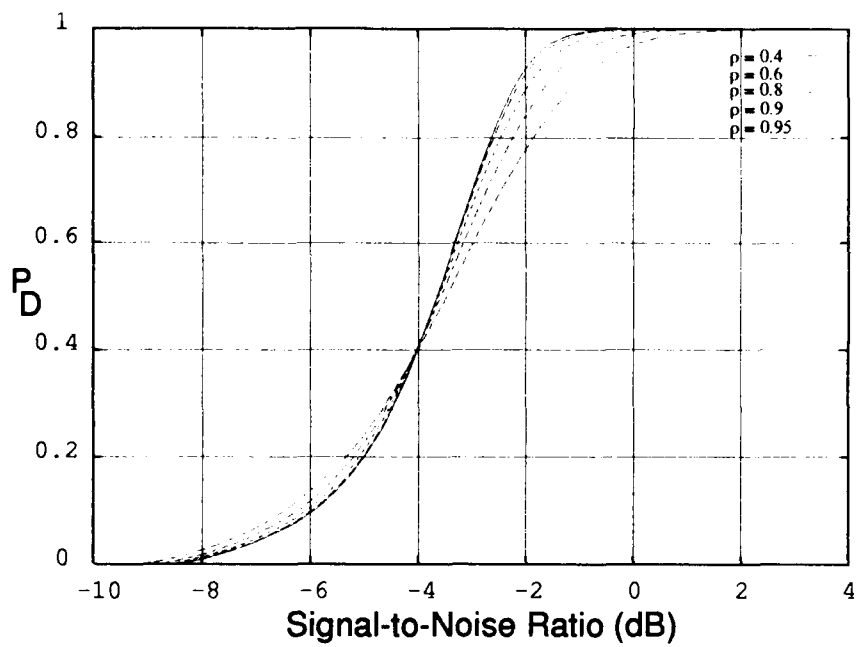
Figure 2.5. Saddlepoint Integration for 150 radar pulses

signal autocovariance matrix eigenvalues in a convenient manner. If the number of integrated pulses is less than 150 then the eigenvalues can also be determined by the IMSL fortran subroutine DEVCSF described in section 2.6.3. I used this subroutine to determine the covariance matrix eigenvalues with individual elements described by a $(\sin x/x)^2$ correlation parameter. P_D was then calculated with these eigenvalues and the results we⁻ compared to the P_D calculated with exponential parameter eigenvalues. The two different parameters yielded approximately the same P_D for all of the cases considered. This result indicates that P_D is primarily determined by how fast the correlation parameter first approaches zero and not on the behavior of the correlation parameter beyond this zero value.

2.6.7 Summary In this chapter we have introduced several techniques for determining the probability of detection of Rayleigh distributed radar returns. The original work of Peter Swerling (18) provides the theoretical background for determining P_D of partially correlated signals but does not provide an effective technique for calculating the required covariance matrix eigenvalues. A technique for determining the eigenvalues is given by Irving Kanter (14); however, summation errors limit the number of integrated pulses to 30. This limitation is corrected through the use of saddlepoint integration techniques introduced by Carl Helstrom (10). These models were then used to illustrate the importance of the correlation parameter ρ in determining P_D. For the all the cases considered and for $P_D > 0.4$, the more fluctuating targets required a lower signal-to-noise ratio to achieve the same P_D. In addition, the results of this chapter shows that it is not possible to accurately deter-mine P_D without considering the pulse-to-pulse correlation of the individual radar returns.

III. Determination of the Target Autocovariance

The pulse detection methods developed in chapter 2 require the pulse-to-pulse correlation of the received signal in order to generate the signal autocovariance matrix. Recall that the de-correlation of the signal may be caused by, among others, the target's rotation relative to the radar's line-of-sight or by changes in the radar frequency. The degree of correlation of the signal amplitude from one observation to the next will determine the detection probability (1). Several pdf's have been proposed to describe target fluctuation statistics (2). Among these are the chi-square family, the Rice family, the log-normal family, the Swerling models, and the Weinstock distributions. The Swerling's techniques described in chapter 2 (19) using completely correlated or completely un-correlated pulse-to-pulse signals can be applied to all the above models and for arbitrary pdf's, but extensive numerical calculations have been made only for the original Swerling pdf models. In addition, these calculations do not account for the pulse-to-pulse correlation of the received signal (2).

This chapter develops the analytic models to predict the autocovariance matrix of the received signal. Once the analytic models are developed, it will be possible to determine P_D using the results from the models and the prediction techniques of chapter 2. The first section develops a method of determining the signal autocorrelation function, and is based on the preliminary work of Byron Welsh, et.al. (20). Using the results from this model, we will generate the autocorrelation function for two different types of complex scattering targets. The final section of this chapter gives an empirical approach for estimating the autocovariance matrix.

3.1 Autocovariance of a Complex Target

The following results closely follow the preliminary work performed by Byron Welsh, et.al. (20) on RCS correlation modeling. Their work will permit us to develop the pulse-to-pulse autocorrelation function for an arbitrary distribution of scattering

3-1

centers. A spatial distribution of scatterers can be used to reproduce the scattering statistics expected from a complex target, where the term complex refers to the type of scattering expected from a target consisting of many scattering centers. The spatial extent of the scattering centers is assumed to be large compared to the wavelength of the incident electro-magnetic field. Since the spatial extent is large, the RCS aspect angle pattern will be highly fluctuating and the RCS statistics can be determined from the distribution of the scattering centers. In addition, the use of spatially distributed scatterers will allow us calculate the target autocovariance in a relatively simple manner. We will consider two spatial distribution of scatterers for this analysis. The first distribution is for a collection of scatterers where the individual scatterers have a Gaussian distribution about a set of fixed locations. This distribution requires detailed information about the target scattering centers and should accurately predict the target autocorrelation function. The second distribution considered is where the scattering centers are uniformly distribution within a rectangular box. This distribution was chosen since only the maximum target dimensions are required. These maximum dimensions correspond to the dimensions of the box. Since only the maximum dimensions are required, it is relatively easy to predict the autocovariance of the target using this distribution. Remember that we would like to predict the autocovariance using the simplest model possible. We will then compare the uniform distribution predictions to the point source distributions. If the two prediction methods agree, we will then be able to use the much simpler uniform distribution technique to calculate the target autocovariance.

The target and observer geometry used throughout this section is illustrated in Fig 3.1. The following definitions will be used through this section to describe the quantities of interest:

$\vec{r}_i$ = vector position of the ith point scatterer

$\underline{b}_i(\hat{r})$ = scaler backscattered field from the ith point scatterer for a unit amplitude incident field
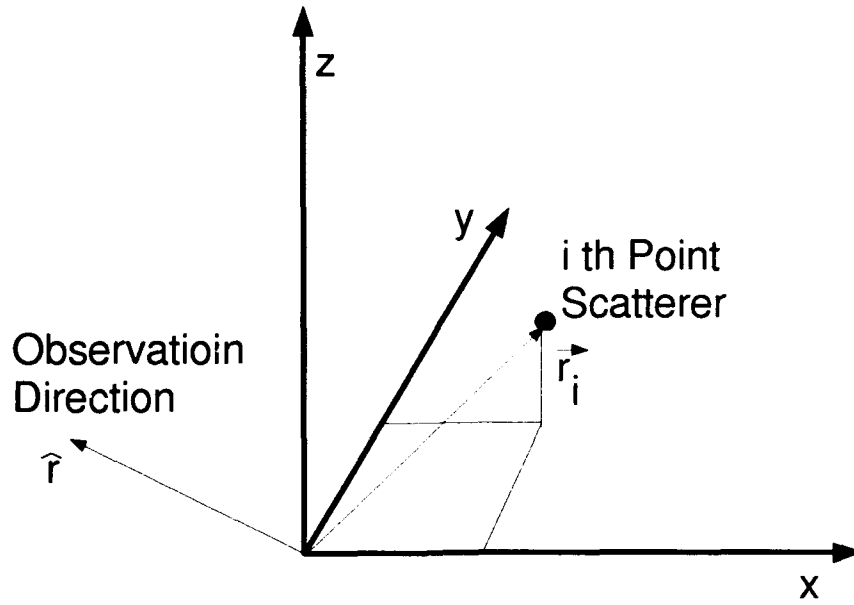
Figure 3.1. Target/Observer Geometry

$\hat{r}$ = unit vector pointing in the direction of the observation point,

$\underline{y}(\hat{r})$ = complex amplitude of the total scattered E field,

λ = wavelength of the incident and scattered field.

The expression for the complex amplitude of the scattered field is given as

$$\underline{y}(\hat{r}) = \sum_{i=1}^{N} \underline{b}_i(\hat{r}) \exp\left\{ j\frac{4\pi}{\lambda}(\hat{r} \cdot \vec{r}_i) \right\}, \qquad (3.1)$$

where N is the number of scatterers in the observation direction $\hat{r}$. The power of the scatterer field in the $\hat{r}$ direction is proportional to the squared magnitude of the scattered field:

$$\sigma(\hat{r}) = | \underline{y}(\hat{r}) |^2 = \sum_{i=1}^{N} \sum_{i'=1}^{N} \underline{b}_i(\hat{r})\underline{b}_{i'}^{*}(\hat{r}) \exp\left\{ j\frac{4\pi}{\lambda}[\hat{r} \cdot (\vec{r}_i - \vec{r}_{i'})] \right\}. \qquad (3.2)$$

The autocorrelation of σ is required to calculate P_D and is given as

$$
\begin{aligned}
R_\sigma(\hat{r}_1, \hat{r}_2) &= E[\sigma(\hat{r}_1)\sigma(\hat{r}_2)] \\
&= E[|\ \underline{y}(\hat{r}_1)\ |^2 |\ \underline{y}(\hat{r}_2)\ |^2]
\end{aligned}
\tag{3.3}
$$

where $R_\sigma(\hat{r}_1, \hat{r}_2)$ is the autocorrelation function and $E[\ \ ]$ is the expected value operator. As will be discussed later, the individual elements of the signal covariance matrix C are generated from this autocovariance function.

3.1.1 Assumptions

The following assumptions are made to simplify the analysis.

$\underline{b}_i(\hat{r}) = \underline{b}_i$.

$|\ \underline{b}_i\ |$ is independent of $\arg[\underline{b}_i]$.

$\arg[\underline{b}_i]$ is uniformly distributed over the interval $[0, 2\pi]$.

$\underline{b}_i$ and $\vec{r}_i$ are independent.

3.1.2 Implications

The assumptions listed in the preceding section results in the following implications:

$$
E[\underline{b}_i] = 0,
\tag{3.4}
$$

$$
E[\underline{b}_i^2] = 0,
\tag{3.5}
$$

$$
E[\underline{b}_i \underline{b}_{i'}^*] = \begin{cases} \alpha^2 & i = i', \\ 0 & i \neq i' \end{cases}
\tag{3.6}
$$

Using the above assumptions, the expected value of $\sigma(\hat{r})$ is given by

$$
E[\sigma(\hat{r})] = N\alpha^2,
\tag{3.7}
$$

3-4

which agrees with the value determined by Crispen (3), for the incoherent addition of scatterers. Using the above assumptions, the autocorrelation function can be expressed as

$$R_\sigma(\hat{r}_1, \hat{r}_2) = E\left[\sum_{i=1}^{N}\sum_{i'=1}^{N}\sum_{n=1}^{N}\sum_{n'=1}^{N} \underline{b}_i\underline{b}_{i'}^*\underline{b}_n\underline{b}_{n'}^* \times \exp\left\{j\frac{4\pi}{\lambda}[\hat{r}_1 \cdot (\vec{r}_i - \vec{r}_{i'}) + r_2 \cdot (\vec{r}_n - \vec{r}_{n'})]\right\}\right].$$

Since $\underline{b}_i$ and $\vec{r}_i$ are independent, the quantity $E[\underline{b}_i\underline{b}_{i'}^*\underline{b}_n\underline{b}_{n'}^*]$ can be considered separately. Using eqn's 3.4 thru 3.6, it is easy to show:

$$E[\underline{b}_i\underline{b}_{i'}^*, \underline{b}_n\underline{b}_{n'}^*] = \begin{cases} E[|\underline{b}_i|^4] & i = i' = n = n' \\ \alpha^4 & i = i' \text{ and } n = n' \text{ and } i \neq n \\ \alpha^4 & i = n' \text{ and } n = i' \text{ and } i \neq i' \\ 0 & \text{otherwise} \end{cases} \tag{3.8}$$

Using eqn 3.8, the autocorrelation function can be written as:

$$\begin{aligned} R_\sigma(\hat{r}_1, \hat{r}_2) &= NE[|\underline{b}_i|^4] + N^2\alpha^4 - 2N\alpha^4 \\ &+ \alpha^4 \sum_{i=1}^{N}\sum_{i'=1}^{N}\left\{E\left[\exp\left\{j\frac{4\pi}{\lambda}[(\hat{r}_1 - \hat{r}_2) \cdot (\vec{r}_i - \vec{r}_{i'})]\right\}\right]\right\}. \end{aligned} \tag{3.9}$$

Equation 3.9 can be further simplified by recognizing that the expected value in the fourth term can be written in terms of the characteristic function of $\vec{r}_i$. The characteristic function for a random process $\vec{u}$ is given as

$$\underline{M}_{\vec{u}}(\vec{\omega}) = E[e^{j\vec{\omega}\cdot\vec{u}}], \tag{3.10}$$

where $\vec{\omega}$ is a vector of the same dimension as $\vec{u}$ (4). The characteristic function can also be written in terms of an inverse Fourier transform operation. If $\vec{u}$ is of dimension n, we can write the characteristic function as

$$\underline{M}_{\vec{u}}(\vec{\omega}) = (2\pi)^2 F_n^{-1}[p_u(2\pi\vec{u})], \tag{3.11}$$

where $p_u(\vec{u})$ is the probability density function (pdf) of $\vec{u}$ and F_n^{-1} is the n-dimensional inverse Fourier transform operator. The Fourier transform operators are defined as:

$$F_n[p_u(\vec{u})] = \int p_u(\vec{u})e^{(-j2\pi\vec{u}\cdot\vec{\omega})}\mathrm{d}^n\vec{u} \qquad (3.12)$$

$$F_n^{-1}[p_u(\vec{u})] = \int p_u(\vec{u})e^{(j2\pi\vec{u}\cdot\vec{\omega})}\mathrm{d}^n\vec{u} \qquad (3.13)$$

Using the results given in equations 3.12 and 3.13 the expected value in the fourth term of eqn 3.9 can be written as

$$E\left[\exp\left\{j\frac{4\pi}{\lambda}\left[(\hat{r}_1 - \hat{r}_2)\cdot(\vec{r}_i - \vec{r}_{i'})\right]\right\}\right] = F_n[F_n^{-1}[p_{i|i'}^r(\vec{r}_i \mid \vec{r}_{i'})]|_{\vec{\omega}=\frac{2}{\lambda}\vec{\Delta}_r}\, p_{i'}^r(\vec{r}_{i'})]|_{\vec{\omega}=\frac{2}{\lambda}\vec{\Delta}_r}, \qquad (3.14)$$

where $p_i^r(\vec{r})$ is the pdf of $\vec{r}_i$, $p_{i|i'}^r(\vec{r}_i \mid \vec{r}_{i'})$ is the conditional pdf of $\vec{r}_i$ given $\vec{r}_{i'}$. The directional change in the observation point ($\vec{\Delta}_r$) is defined by $\vec{\Delta}_r \doteq \hat{r}_1 - \hat{r}_2$. Using the above results eqn 3.9 can be rewritten as

$$\begin{aligned}
R_\sigma(\vec{\Delta}_r) &= NE[|\,\underline{b}_i\,|^4] + N^2\alpha^4 - 2N\alpha^4 \\
&\quad + \alpha^4 \sum_{i=1}^{N}\sum_{i=1}^{N} F_n[F_n^{-1}[p_{i|i'}^r(\vec{r}_i \mid \vec{r}_{i'})]]p_{i'}^r(\vec{r}_{i'})]|_{\vec{\omega}=\frac{2}{\lambda}\vec{\Delta}_r}.
\end{aligned} \qquad (3.15)$$

Assuming the real and imaginary of $\underline{b}_i$ are Gaussian implies that the $|\,\underline{b}_i\,|$ is Rayleigh distributed, which is consistent with an earlier assumption concerning the signal pdf given in chapter 2. The first term in eqn 3.15 can be shown to be

$$E[|\,\underline{b}_i\,|^4] = 2\alpha^4. \qquad (3.16)$$

Using this assumption, eqn 3.15 can now be written as

$$R_\sigma(\vec{\Delta}_r) = N^2\alpha^4 + \alpha^4 \sum_{i=1}^{N}\sum_{i'=1}^{N} F_n[F_n^{-1}[p_{i|i'}^r(\vec{r}_i \mid \vec{r}_{i'})]]p_{i'}^r(\vec{r}_{i'})]|_{\vec{\omega}=\frac{2}{\lambda}\vec{\Delta}_r} \qquad (3.17)$$

If the position of the ith scatterer is independent of the position of the i' scatterer, then eqn 3.17 is given as

$$R_\sigma(\vec{\Delta}_r) = N^2\alpha^4 + \alpha^4 \sum_{i=1}^{N} \sum_{i'=1}^{N} [F_n^{-1}[p_i^r(\hat{r}_i)]]_{\bar{\omega}=\frac{2}{\lambda}\vec{\Delta}_r} \cdot [F_n[p_{i'}^r(\hat{r}_{i'})]]_{\bar{\omega}=\frac{2}{\lambda}\vec{\Delta}_r}$$

$$= N^2\alpha^4 + \alpha^4 \left| \sum_{i=1}^{N} F_n^{-1}[p_i^r(\hat{r}_i)]_{\bar{\omega}=\frac{2}{\lambda}\vec{\Delta}_r} \right|^2 . \tag{3.18}$$

The autocovariance is determined by subtracting the mean squared value of σ from the autocorrelation function (4). Thus, the autocovariance can be written as:

$$K_\sigma(\vec{\Delta}_r) = \alpha^4 \left| \sum_{i=1}^{N} F_n^{-1}[p_i^r(\hat{r}_i)]_{\bar{\omega}=\frac{2}{\lambda}\vec{\Delta}_r} \right|^2 . \tag{3.19}$$

This general model allows us to calculate the signal autocovariance for any given scattering center distribution, $p_i^r(\hat{r})$. The autocovariance is then used to determine P_D using the radar detection model of chapter 2. The next step is to calculate the signal autocovariance for a given distribution of scattering centers. The first distribution considered is where the individual scatterers have a Gaussian distribution about a collection of fixed points in the xy plane. This distribution is chosen since the location and magnitude of the scattering centers can be easily determined from a two dimensional radar image of the target. The second distribution considered is a uniform distribution of scattering centers in a rectangular area of the xy plane. The rectangular scattering center distribution is chosen since the only knowledge required for the calculation of the autocovariance function are the x and y dimensions of the target.

3.1.3 Point Source Scattering Centers The first autocorrelation function we will generate using the above model is for a collection of scattering centers where each scattering center has a Gaussian distribution about a fixed location in the xy plane. This distribution is chosen since it requires the most information about the

target's RCS. Specifically, we require the position and magnitude of each scattering center. The pdf of the position of each scatterer is described by:

$$p_i^r(x,y) = \frac{1}{2\pi\sigma_x\sigma_y} \exp\left\{\frac{-1}{2}\left[\left(\frac{x-x_i}{\sigma_x}\right)^2 + \left(\frac{y-y_i}{\sigma_y}\right)^2\right]\right\} \qquad (3.20)$$

where σ_x and σ_y are the standard deviations of the ith scattering center about the means x_i and y_i. The inverse Fourier transform of eqn 3.20 is given by

$$F_2^{-1}[p_r^i(x,y)] = \frac{1}{2\pi\sigma_x\sigma_y} \int\int \exp\left\{\frac{-1}{2}\left[\left(\frac{x-x_i}{\sigma_x}\right)^2 + \left(\frac{y-y_i}{\sigma_y}\right)^2\right]\right\}$$

$$\times \exp(j2\pi(x\omega_x + y\omega_y))dxdy \qquad (3.21)$$

where ω_x and ω_y are the x and y directed components of $\vec{\omega}$. Carrying out the integration of eqn 3.21 gives

$$F_2^{-1}[p_r^i(x_i,y_i)] = \frac{1}{\pi}\exp\left\{-\frac{\omega_x^2\sigma_x^2 + \omega_y^2\sigma_y^2}{2}\right\}\exp\left\{j2\pi\left[(\omega_x x_i + \omega_y y_i]\right\}. \qquad (3.22)$$

Substituting eqn 3.21 into eqn 3.18 gives

$$R_\sigma(\vec{\Delta_r}) = N^2\alpha^4 + \left|\sum_{i=1}^{N} \frac{\alpha_i^2}{\pi}\exp\left\{-\frac{2\Delta_x^2\sigma_x^2 + 2\Delta_y^2\sigma_y^2}{\lambda^2}\right\}\exp\left\{\frac{j4\pi}{\lambda}\left[(\Delta_x x_i + \Delta_y y_i]\right\}\right|^2 \qquad (3.23)$$

Subtracting the mean squared value then gives the autocovariance

$$K_\sigma(\vec{\Delta_r}) = \left|\sum_{i=1}^{N} \frac{\alpha_i^2}{\pi}\exp\left\{-\frac{2\Delta_x^2\sigma_x^2 + 2\Delta_y^2\sigma_y^2}{\lambda^2}\right\}\exp\left\{\frac{j4\pi}{\lambda}\left[\Delta_x x_i + \Delta_y y_i]\right\}\right|^2 \qquad (3.24)$$

The signal covariance matrix can be calculated from the autocovariance. P_D is then calculated using the detection model developed in chapter 2. Before we proceed with the P_D calculations, we will also determine the autocovariance function for a uniform distribution of scattering centers.

3.1.4 Uniform Distribution of Scattering Centers The second scatterer distribution considered is where the N point scatterers are uniformly distributed within a rectangular area of width L_x and length L_y. This distribution was chosen since it requires the least amount of target information. The pdf for this distribution is easily written as

$$p^r(\vec{r}) = \frac{1}{L_x L_y}\text{rect}\left(\frac{x}{L_x}\right)\text{rect}\left(\frac{y}{L_y}\right),\qquad(3.25)$$

where

$$\text{rect}(x) = \begin{cases} 1 & |x| < \frac{1}{2} \\ 0 & \text{elsewhere} \end{cases}\qquad(3.26)$$

Application of the the two-dimensional Fourier transform and simplifications, results in the following autocorrelation function

$$R_\sigma(\vec{\Delta}_r) = N^2\alpha^4\left[1 + \left\{\text{sinc}\left(\frac{2L_x\Delta_x}{\lambda}\right)\text{sinc}\left(\frac{2L_y\Delta_y}{\lambda}\right)\right\}^2\right],\qquad(3.27)$$

where the $\text{sinc}(u) = \sin(u\pi)/u\pi$. The corresponding autocovariance function is given by:

$$K_\sigma(\vec{\Delta}_r) = N^2\alpha^4\left\{\text{sinc}\left(\frac{2L_x\Delta_x}{\lambda}\right)\text{sinc}\left(\frac{2L_y\Delta_y}{\lambda}\right)\right\}^2\qquad(3.28)$$

The point source and uniform distribution models gives us two methods of determining the signal autocovariance. The point source distribution requires the most information about the target and is therefore more difficult to implement than the uniform distribution of scatterers. However, the point source distribution will give an accurate prediction of the autocovariance. The uniform distribution is chosen because only the maximum dimension of the target are required and the autocovariance is therefore easily calculated. Finally, we are interested in comparing the predicted autocovariance, $K_\sigma(\vec{\Delta}_r)$ to an empirically derived autocovariance, $\hat{K}_\sigma(k)$. The two covariance prediction models can then be compared to the empirical estimate to see how different target shapes affect the autocovariance.

3.2 Empirical Estimate of the Autocorrelation Function

An empirical estimate of the signal autocovariance function can be obtained from the measured RCS data. This method is useful if the target RCS pattern is known. The empirical results will then be compared to the autocovariance predictions previously developed. The following empirical estimate of the autocorrelation function is given by Levanon(15) and Crispen (3)

$$\hat{R}_\sigma[k] = \frac{1}{N-k} \sum_{k=0}^{N-1-k} z_k^* z_{n+k}, \quad 0 \le k \le N - 1, \tag{3.29}$$

were z_k is a sequence of target RCS values (m^2). The estimate of the expected value of z is

$$\bar{z} = \frac{1}{N} \sum_{k=0}^{N-1} z_k, \tag{3.30}$$

and the autocovariance estimate is determined by

$$\hat{K}_\sigma = \hat{R}_\sigma[k] - \bar{z}^2. \tag{3.31}$$

3.3 Summary

This chapter has shown how the autocorrelation of the RCS can be predicted for any distribution of scattering centers. The autocovariance was determined for two types of distributions. The uniform distribution is the easiest method to implement since it only requires the maximum dimensions of the the target. The point source distribution requires the location and magnitude of the individual scattering centers and is more difficult to implement but should provide a more accurate estimate of the autocorrelation. Finally, we introduced a method for empirically estimating the autocovariance using the measured RCS data. The next chapter compares these two prediction techniques to the empirical estimate of the autocorrelation for a particular complex target.

IV. Target Model

In chapter 2 we showed the importance of the correlation parameters in determining P_D of a target. In chapter 3 we developed a technique to describe the signal correlation properties based on the target's scattering center distributions. We also introduced an empirical method of estimating the autocovariance using measured RCS data. Our goal is to model the autocovariance of the target without having to revert to the detailed angular sampling of two samples per RCS lobe. With this goal in mind, the next step is investigate how well the autocovariance prediction techniques estimate the autocovariance of the target.

This chapter illustrates how to use the uniform and point source scattering center distribution predictions to calculate the autocovariance of a complex target. The autocovariance is also empirically estimated from the measured RCS data. This estimate is then compared to the two predicted autocovariances discussed in chapter 3. This comparison is made using the RCS from the AIM-9 missile.

4.1 AIM-9 Missile

An AIM-9 missile model is used to show how the autocovariance varies with changes in the observation angle. The 1/3.72 scale model is shown in Figure 4.1. The model was measured at Ohio State University's compact radar range at 36 GHz. The target was measured at a zero degree elevation angle, and in azimuth at every 0.15 degrees from 0 to 180 degrees. The missile was chosen because the spatial extent of the scattering centers are large in the side-on dimension (95 wavelengths), and small in the nose-on dimension (11 wavelengths). The significance of the spatial extent will be shown later. The missile was also chosen since it is a relatively complex target.

The 0 to 180 degrees azimuth RCS plot of the missile at zero degrees elevation is given in Figure 4.2. Note that zero degrees corresponds to the nose-on observation angle, and 90 degrees is the side-on observation angle. As seen from the plot, the

Side View   **Front View**
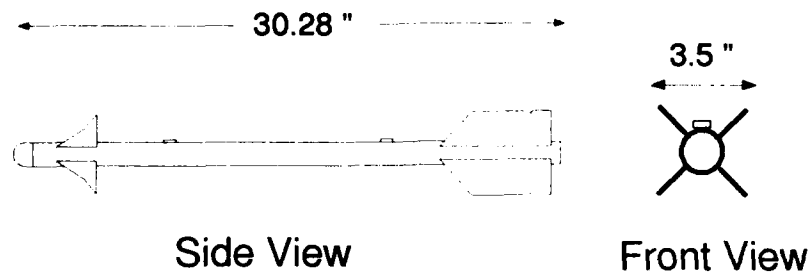
Figure 4.1. AIM-9 Missile

widest lobe width occurs at the nose on aspect angles. The lobes widths become increasingly narrow as the observation angle approaches broadside. The RCS pattern of the target can be more easily seen if the azimuth scale is expanded. A 30 to 60 degrees azimuth plot of the missile is shown in Figure 4.3. Before we proceed further,
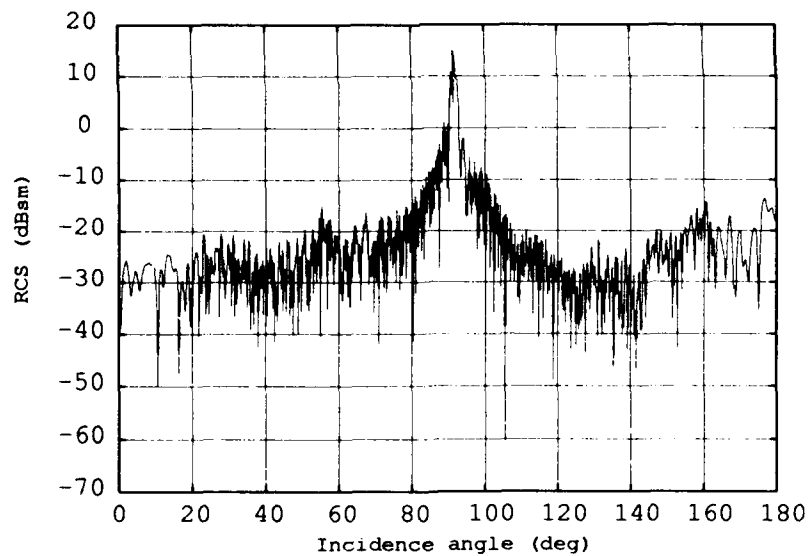
Figure 4.2. 36 GHz, 0° − 180° Missle RCS Azimuth Plot

a brief discussion on the RCS lobing structure will help explain the autocovariance plots shown at the end of this chapter.
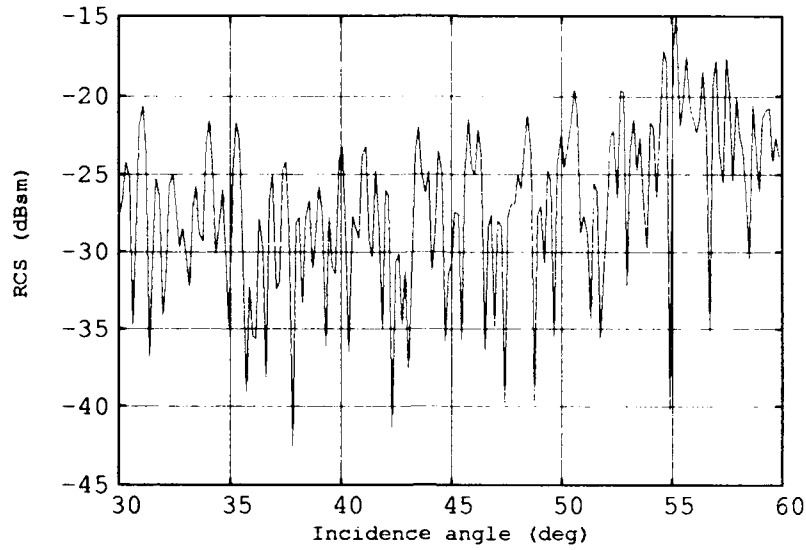
Figure 4.3. 36 GHz, $30° - 60°$ Missle RCS Azimuth Plot

The RCS lobes widths of a complex target can be estimated from our earlier results of chapter 3. Recall the results of chapter 3 showed the target RCS is given as

$$\sigma(\hat{r}) = \left| \sum_{i=1}^{N} \underline{b}_i \exp\left\{ j \frac{4\pi}{\lambda} (\hat{r} \cdot \vec{r_i}) \right\} \right|^2 , \tag{4.1}$$

where $\underline{b}_i$ is the scaler backscattered field from the ith point scatterer for a unit amplitude incident field and $\hat{r}$ is a unit vector pointing in the direction of the observation point. Using the target/observer geometry of Figure 4.4, eqn 4.1 can be written as

$$\sigma(\theta) = \left| \sum_{i=1}^{N} \underline{b}_i e^{\left\{ \frac{j4\pi}{\lambda} (x_i \cos\theta + y_i \sin\theta) \right\}} \right|^2 , \tag{4.2}$$

where θ is the observation angle and is measured from the x-axis and x_i and y_i are the x and y-directed components of $\vec{r_i}$.

The RCS lobe widths can now be explained by examining eqn 4.2. For small changes in the observation angle, $\Delta\theta$, about $\theta = 0°$, the $\cos(\Delta\theta)$ term is approximately equal to one; however, the $\sin(\Delta\theta)$ term is approximately equal to $\Delta\theta$. As

4-3

θ varies by a small amount, the $x_i \cos \theta$ components do not change very quickly compared to the $y_i \sin \theta$ components. The RCS fluctuations are due to the coherent addition of the scattered field for each of the N scattering centers. If $\Delta\theta$ is small, the effects of the scatterers in the x-dimension will be small, and the RCS fluctuations will be determined by the scatterers in the y-dimension. Thus, the RCS lobe widths are determined by the y_i terms in eqn 4.2. At a 90 degree observation angle the cosine terms in eqn 4.2 fluctuate more rapidly than the sine terms and the x_i terms determine the RCS lobe widths.

These results explain the RCS lobing structure of the missile in Figure 4.2. For the 0 degree observation angle, the y-dimension of the scatterers is less than 3.5 inches. As θ is varied, the coherent addition of the scattered field changes slowly, since the y-dimension of the scatterers is small. At a 90 observation angle, the x-dimension of the scatterers is 30.28 inches, almost 10 times larger than the y-dimension, and the resultant RCS lobe widths are about 10 times smaller than the 0 degree observation angle.

4.2 AIM-9 Missile Autocovariance Predictions

The location and relative magnitude of the missile scattering centers were determined from a radar image of the missile. The location of the scattering centers are shown in Figure 4.4 and Table 4.1.

Table 4.1. Locations of the Scattering centers at a 45° Observation Angle

Scatterer Number	Magnitude (dBsm)	x-Axis Location	y-Axis Location
1	-29.1	15.3 in	0.5 in
2	-40.5	11.1 in	1.28 in
3	-41.9	10.4 in	1.71 in
4	-40.8	-4.2 in	0.5 in
5	-36.8	-15. in	0.67 in
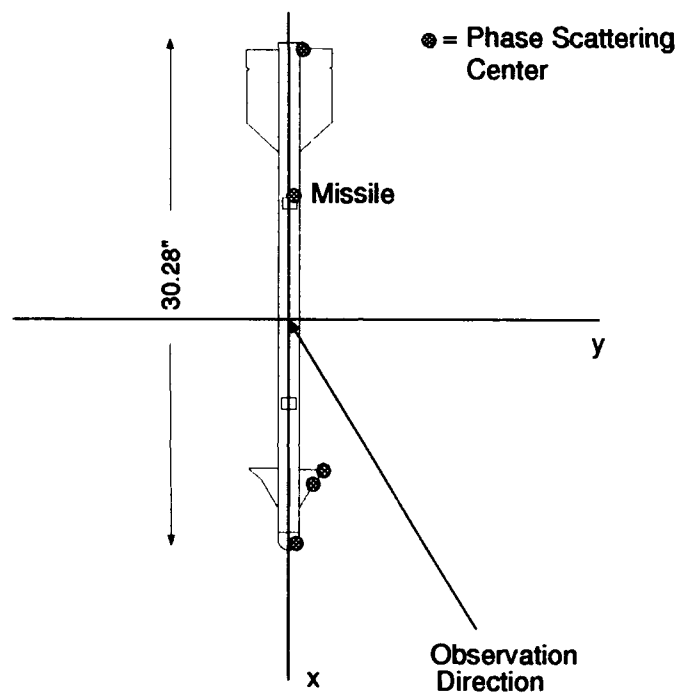
Figure 4.4. Scattering Center Locations at a 45° Observation Angle
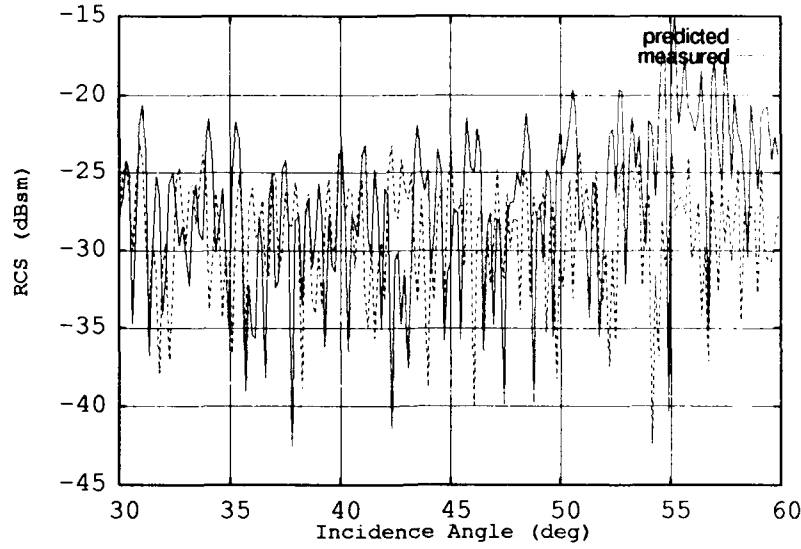
Figure 4.5. Predicted and Measured RCS Azimuth Patterns

The predicted RCS using the point source model was then compared to the measured RCS pattern. The measured RCS and the predicted RCS patterns are shown in Figure 4.5. As seen in the plot, the point source model provides an acceptable approximation to the RCS lobing structure for the missile. The autocovariance function is then determined by eqn 4.3 and the point source scattering locations in Table 4.1. Using eqn 3.24 the autocovariance of the point source distribution is givenen as

$$K_\sigma(\vec{\Delta_r}) = \left| \sum_{i=1}^{N} \frac{\alpha_i^2}{\pi} \exp\left\{ -\frac{2\Delta_x^2\sigma_x^2 + 2\Delta_y^2\sigma_y^2}{\lambda^2} \right\} \exp\left\{ \frac{j4\pi}{\lambda} [\Delta_x r_i + \Delta_y y_i] \right\} \right|^2 . \qquad (4.3)$$

where $N = 5$ and the locations x_i and y_i correspond to the values in Table 4.1.

The second scattering model is the uniform distribution of scattering centers. Recall from chapter 3 that the autocovariance for this distribution function is given by:

$$K_\sigma(\vec{\Delta_r}) = N^2\alpha^4 \left\{ \text{sinc}\left(\frac{2L_x\Delta_x}{\lambda} \right) \text{sinc}\left(\frac{2L_y\Delta_y}{\lambda} \right) \right\}^2 \qquad (4.4)$$

The missile target dimensions L_x and L_y are given as 30.28 inches and 3.5 inches respectively.

4.3 Autocovariance of the AIM-9 Missile at 30, 40, and 45 degrees

The RCS autocovariance is also empirically estimated using the measured RCS data and eqn's 3.29 to 3.31. The autocovariance is calculated for three different observation directions. We will define the de-correlation angle to be the width of the first or main lobe in autocovariance plots. Recall that the de-correlation of the received signal is determined by the RCS lobing structure of the target, i.e. narrower RCS lobes correspond to smaller de-correlation angles. The predicted autocovariance results are shown in figures 4.6 to 4.8.
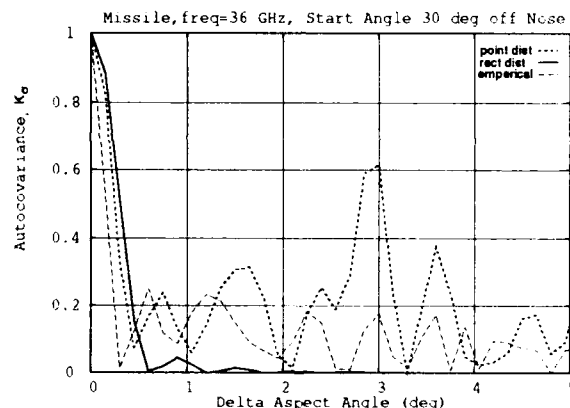
Figure 4.6. Signal Autocovariance, 30 deg off Nose, 5 Scatters

As can be seen from the autocovariance plots the point source distribution and the uniform distribution predictions agree fairly well for all three observation angles. For each of the three cases the point source prediction provides a slightly smaller de-correlation angle than the uniform distribution. For the 30 degree observation angle, the autocovariance based on the measured data provides a smaller de-correlation angle than either the point source or uniform distribution prediction. Recall that the point source locations were determined by a radar image of the target at a 45

4-7
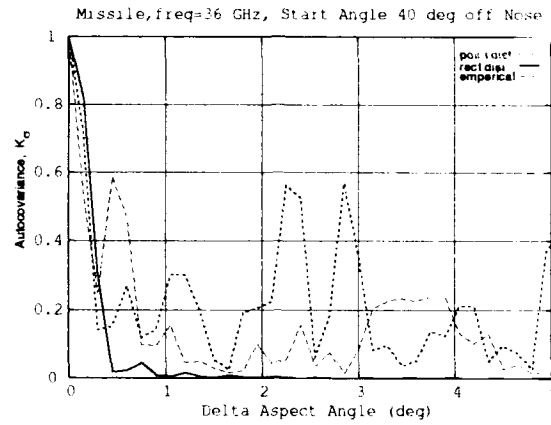
Figure 4.7. Signal Autocovariance, 40 deg off Nose
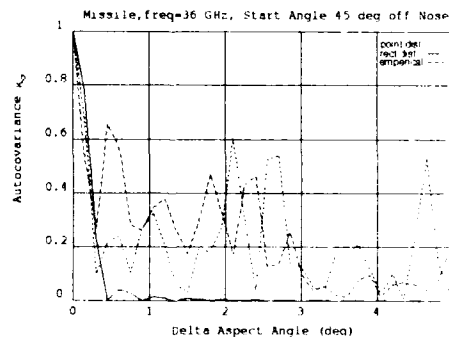
Figure 4.8. Signal Autocovariance, 45 deg off Nose

degree observation angle. As shown in Figure 4.8, the two predicted autocovariances and the empirical estimate give the same de-correlation angle of 0.5 degrees.

4.4 Autocovariance of the AIM-9 Missile at 0, 10, and 30 degrees

The autocovariance was also calculated for the nose-on observation angles. For the point source distribution prediction, the scattering center locations are shown in Table 4.2. For this case, the scattering center locations were also determined from a radar image of the target. The autocovariance was determine for observation directions of 0, 10, and 30 degrees off the nose of the missile. The resultant autocovariance plots are shown in Figure 4.9, 4.10, and 4.11.

Table 4.2. Locations of the Scattering centers at a 0° Observation Angle

Scatterer Number	Magnitude (dBsm)	x-Axis Location	y-Axis Location
1	-40.8	15.3 in	0 in
2	-39.8	10.4 in	1.17 in
3	-46.2	2.8 in	.5 in
4	-38.0	-5.2 in	0.5 in
5	-46.8	-11.6 in	0.5 in
6	-52.2	-8.0 in	0.5 in
7	-35.1	-14.5 in	.67 in
8	-39.6	-13.3 in	1.89 in
9	-39.8	10.4 in	-1.71 in
10	-46.2	2.8 in	-.5 in
11	-38.0	-5.2 in	0.5 in
12	-46.8	-11.6 in	-.5 in
13	-52.2	-8.0 in	-.67 in
14	-35.1	-14.5 in	-1.89 in
15	-39.6	-13.3 in	-1.89 in

For all of the cases considered, the widest de-correlation angle is for the 0 degree observation angle. Figure 4.9 shows the autocovariance for this case. The de-correlation angle is approximately 2.5 degrees. The nose-on autocovariance should have the widest de-correlation angle, since the cross range extent of the target is only
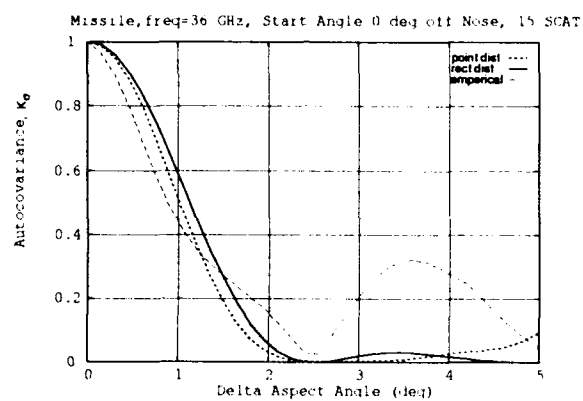
Figure 4.9. Signal Autocovariance, 0 deg off Nose
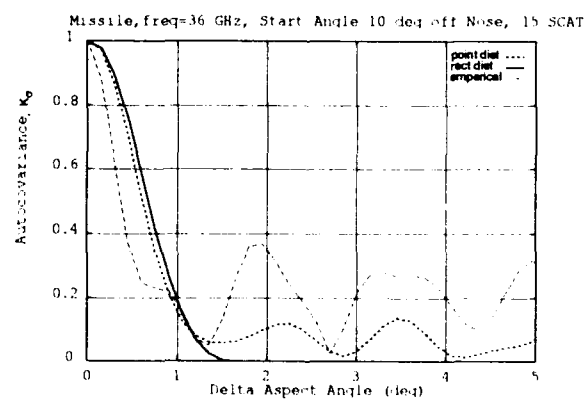
Figure 4.10. Signal Autocovariance, 10 deg off Nose
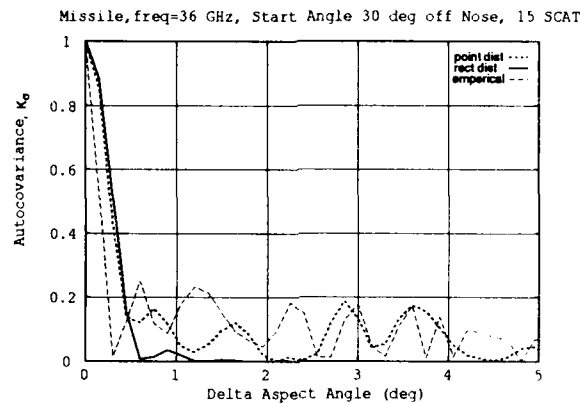
Figure 4.11. Signal Autocovariance, 30 deg off Nose, 15 Scatters

3.5 inches. Remember that the RCS lobe widths are inversely proportional to the cross range extent of the target. Since 0 degrees is the smallest cross range extent, the RCS lobes will be wider and the received signal will fluctuate slower about this observation angle.

For the 0 degree observation angle all three prediction methods provide the same de-correlation angle. Figures 4.9 to 4.11 also illustrate how the de-correlation angle decreases as the observation angle changes from 0 degrees to 30 degrees. For each of the three cases, the point source distribution prediction and the uniform distribution prediction yield approximately the same de-correlation angle, and the empirical estimate yields a slightly smaller de-correlation angle for the 10 degree and 30 degree observation angle cases.

It is also interesting to compare Figure 4.6 to Figure 4.11. For Figure 4.6 the point source locations shown in Table 4.1 were used. The point source locations for Figure 4.11 are from Table 4.2. As shown in the two tables, the distributions differ considerably, 5 scattering centers vs 15 scattering centers; however, the autocovariance plot are approximately the same. Using this observation, it seems reasonable to conclude that a precise determination of the scattering centers is not required to predict the autocovariance properties.

4.5 Summary

This chapter has shown how the correlation prediction techniques of chapter 3 are used to determine the autocovariance function for a complex target. For the cases considered, we found the uniform distribution yields approximately the same de-correlation angle as the point source distribution. For other types of targets this might not be the case. The empirical estimate of the autocovariance yields smaller de-correlation angles than the two predictions. In addition, the uniform distribution provides approximately the same de-correlation angle as the point source distribution. Recall that the point source prediction requires the location and relative magnitude of the target scattering centers. Determining the location and magnitude of the scattering centers of a complex target is not easy. The uniform distribution requires only the maximum dimensions of the target and the autocovariance is easily calculated for this type of distribution.

V. Concluding Examples

We are now ready to show how the P_D detection model of chapter 2 and the autocorrelation prediction models of chapters 3 and 4 can be combined to determine P_D for a given radar/target engagement. The results of this chapter will again emphasize the importance of the correlation parameter, ρ, in determining P_D.

We begin this example by defining the target/radar geometry. Once the flight geometry is defined, the correlation parameter ρ is determined from the target autocovariance predictions of chapter 4. P_D is then calculated from the eigenvalues of the signal covariance matrix, using the saddlepoint integration method of chapter 2.
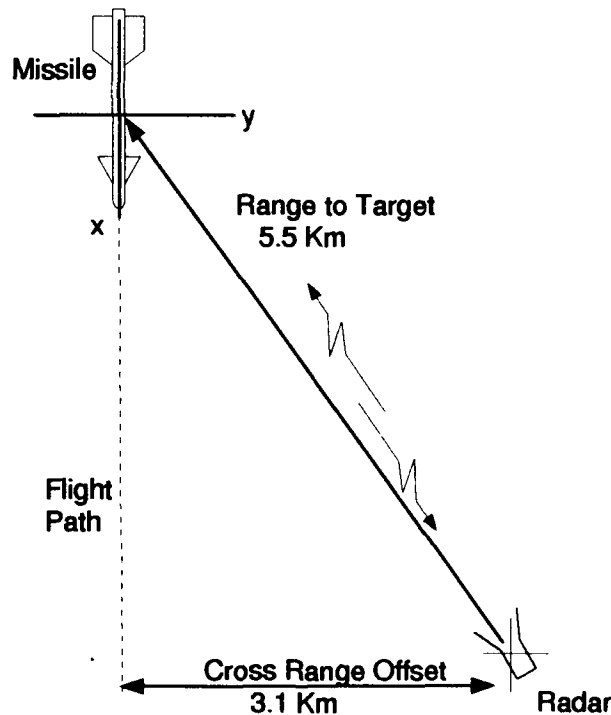

Figure 5.1. Missile/Radar Engagement Geometry

The target/radar engagement geometry is shown in Figure 5.1. The missile's initial position is at 4.5 km down range and 3.1 km cross range from the radar. The velocity of the missile is set at 600 mph (268 m/s), and the missile flies pass the radar maintaining the 3.1 km cross range offset. The missile and radar are at the same altitude, and the pulse repetition frequency of the radar is chosen to be 40 Hz. The probability of false alarm, P_{FA}, is given as 10^{-6}.

For this example, three arbitrary integration intervals were used to illustrate how to calculate P_D using the prediction techniques of chapter 2. The first interval is one second, or 40 integrated pulses. The second interval is 3 seconds (120 pulses), and the third interval is 3.75 seconds (140 pulses). For each of the three cases the initial geometry is shown in Figure 5.1. For this geometry, the initial radar observation angle is 30 degrees off the nose of the missile.

For the 1 second integration interval, the observation angle changes from 30 degrees to 36.7 degrees, as the missile flies pass the radar. The final observation angles for the 3 sec and 3.75 sec integration intervals are 40.5 and 42.1 degrees respectively. Figure 5.2 shows the RCS azimuth plot of the missile for a 30 to 60 degree observation angle.

The autocovariance was calculated using the point source distribution for the scattering center locations given in Table 4.1, and the uniform rectangular distribution model described in chapter 4. The resultant autocovariance functions are shown in Figure 5.3.

Recall that Kanter (14) assumes a single parameter ρ to describe the pulse-to-pulse correlation. This assumption allows the signal autocovariance matrix eigenvalues to be computed in a convenient manner. The criteria for choosing this correlation parameter is somewhat arbitrary. For this analysis, the correlation parameter is defined in the following manner. Referring to figure 5.3, it is easy to see that the autocorrelation approaches zero between 0.5 and 1.0 degrees. The de-correlation angle is defined to be the angle where the autocovariance equals 0.05. To illustrate
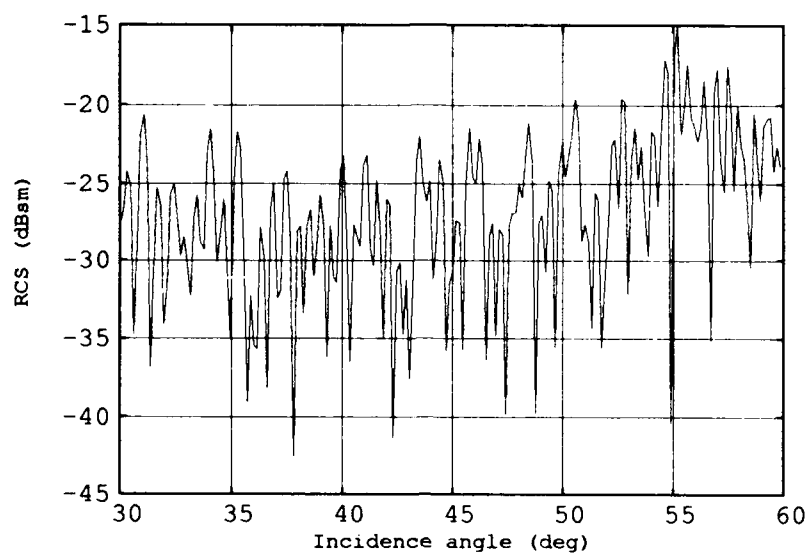
Figure 5.2. Missile RCS Azimuth Plot
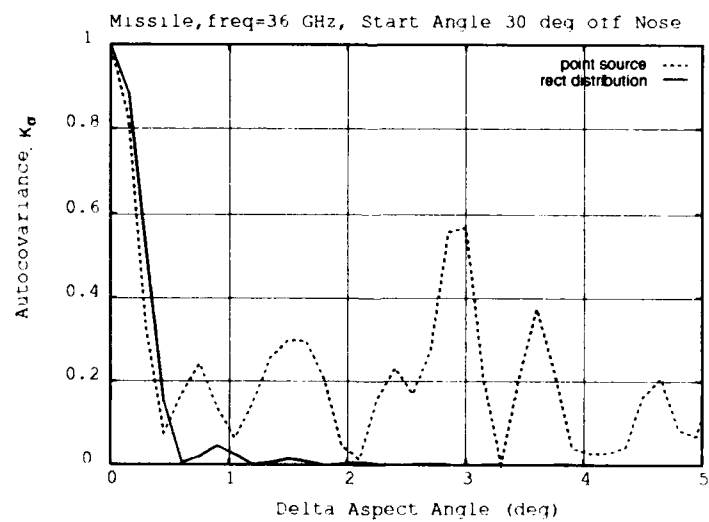
Figure 5.3. Autocovariance for 30 Degrees off Nose

the sensitivity of P_D to the correlation parameter, two additional de-correlation angles of 0.75 and 1.0 degrees were chosen. The pulse-to-pulse exponential correlation parameter, ρ, is determined from the de-correlation angle by

$$\rho = 0.05^{\frac{1}{t_\theta \mathrm{prf}}}, \tag{5.1}$$

where t_θ is the time for the target to rotate through the de-correlation angle, and prf is the pulse repetition frequency of the radar. Using the above method and the missile/radar engagement geometry described earlier, the de-correlation angles of 0.5, 0.75, and 1.0 degrees correspond to pulse-to-pulse exponential correlation parameters of 0.78, 0.84, and 0.88 respectively. Using these correlation parameters, P_D is calculated for each of the three integration intervals. These results are shown in Figures 5.4, 5.5, and 5.6.
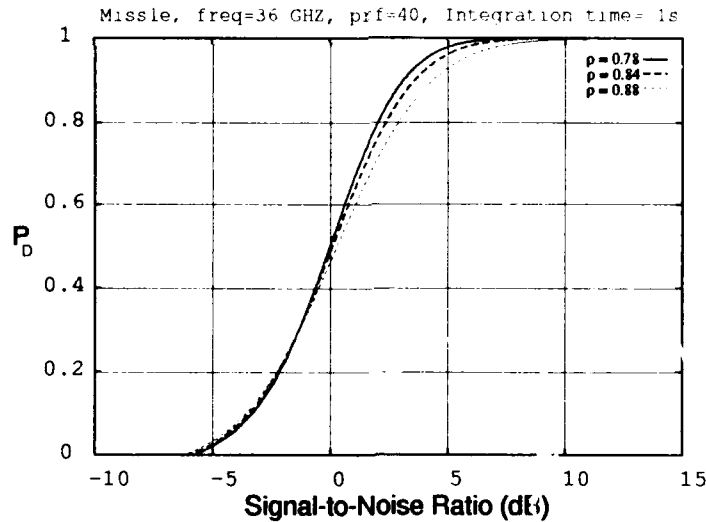
Figure 5.4. *Pd* for 1 sec Observation Time

Again, for we see the same type of results that we saw in chapter 2. Recall that the more rapidly fluctuating targets have a smaller correlation parameter. For P_D less than 0.4, the correlation parameter has only a marginal effect on the determination of

Missle,freq=36GHz, prf=40, Integration time=3s
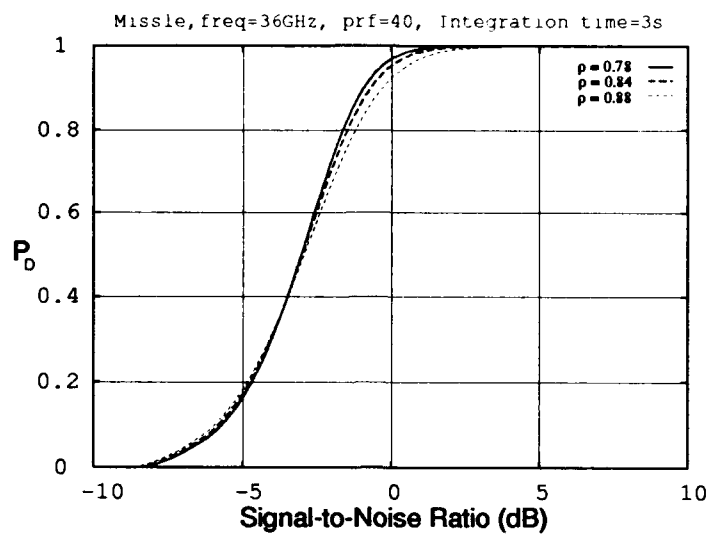
Figure 5.5. *Pd* for 3 sec Observation Time

Missle,freq=36GHZ, prf=40, Integration time=3.75s
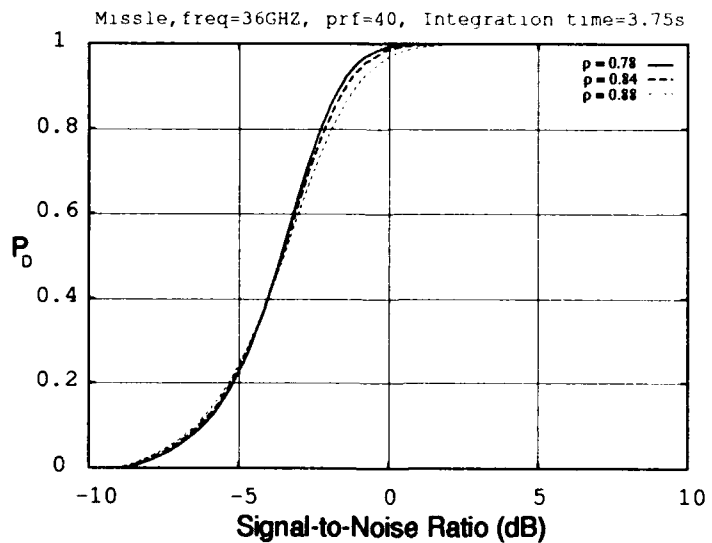
Figure 5.6. *Pd* for 3.75 sec Observation Time

P_D. For values of P_D greater than 0.4, the correlation parameter becomes important in determining P_D.

Consider the 1 sec integration interval case and $P_D = 0.95$. The less fluctuating signal, $\rho = 0.88$, requires and 1.5 dB higher signal-to-noise ratio to achieve the same P_D as the more fluctuating signal of $\rho = 0.78$. Figures 5.5 and 5.6 also show that the less fluctuating signals required higher signal-to-noise ratios to achieve the same P_D.

The above example illustrates how the detection and correlation models from chapters 2 and 3 can be used to determined the P_D for a given target/radar engagement. This example also illustrates the importance of modeling the correlation properties in determining P_D.

VI. Conclusions

In chapter 2 we showed how the detection of correlated radar returns could be computed. The correlated radar return detection was provided by Swerling (18); however, the required signal covariance eigenvalues are not easily calculated. Kanter (14) provided a convenient means for determining these eigenvalues using an exponential correlation parameter; however, summation errors limited the number of integrated pulses to less than 30. This limitation was overcome through the use of saddlepoint integration and the associated saddlepoint approximations introduced by Carl Helstrom (10). The importance of the correlation parameter ρ in determining P_D was then shown using these techniques.

Chapter 3 provided us with several methods for predicting the signal autocovariance function. The autocovariance is determined by the inverse Fourier transform of the target scattering center distribution. The two distributions we concentrated on were a point source and a uniform distribution; however, other types of distributions could also be used. In-addition, we showed how the autocovariance could be empirically estimated from the measured RCS data.

The autocovariance was then predicted for an AIM-9 missile using the techniques described in chapter 3. For this target, the point source and uniform distributions yielded the same de-correlation angle for all the aspect angles considered. Finally, P_D was calculated for the missile using the detection techniques of chapter 2. The results of these calculations once again illustrates the importance of the correlation parameter in determining P_D.

6.1 Follow-on Efforts

The first follow-on effort to this thesis should be to use the detection and correlation prediction techniques to determine the angular RCS sampling requirements.

Additionally, the partially correlation detection techniques could be used to determine how the shape of the autocovariance function affects P_D.

The autocovariance prediction techniques should be applied to other types of targets, to determine if the point source and uniform distributions are the best distributions for predicting the autocovariance.

Appendix A. *Derivation of L(s)*

The derivation for the calculating the Laplace transform of $G(v)$ closely follows the original work of Peter Swerling (18). This derivation is included because it provides us with a method for calculating the P_D of partially correlated radar return signals. The radar receiver model and assumptions on the signal statistics are given in chapter 2. Recall that before we can calculate P_D, we first manipulate $G(v)$ into a form which can be integrated. To do this, we first take the Laplace transform, $L(s)$, of the integrated output pdf $G(v)$, which is given as

$$L(s) = \int_0^\infty e^{-sv} G(v) dv. \tag{A.1}$$

The in-phase and quadrature channel detector outputs, x_i and y_i, are defined by the random vectors U^x and U^y as

$$U_x \doteq (x_1, \cdots, x_N) \qquad U_y \doteq (y_1, \cdots, y_N). \tag{A.2}$$

We will also assume that U_x and U_y are mutually statistically independent. U_x and U_y will have identical signal covariance matrixes, C, with individual elements $c_{i,j}$:

$$c_{i,j} = E[z_i z_j], \qquad i = 1 \cdots N, \qquad j = 1 \cdots N, \tag{A.3}$$

where $E[]$ is the expectation operator. In-addition, the detector output for the ith pulse is assumed to have a Rayleigh pdf described by

$$p(z_i) = \frac{1}{\bar{z}} \exp\left(-\frac{z_i}{\bar{z}}\right). \tag{A.4}$$

The Laplace transform of $G(v)$ can be computed by first considering the conditional pdf for v. The Laplace transform of this conditional pdf is given by the well known

transform (18)

$$L(s \mid v) = \frac{1}{(1+s)^N} \prod_{i=1}^{N} \exp\left[\frac{-s}{1+s}(x_i^2 + y_i^2)\right]. \tag{A.5}$$

The Laplace transform of $G(v)$, $L(s)$, is equal to this expression averaged over the probability distributions of U_x and U_y. Using the mutual independence of the random vectors U_x, U_y, the Laplace transform can be written as

$$L(s) = \frac{1}{(1+s)^N} \int\int \exp\left[-\sum_{i=1}^{N} \frac{s}{1+s}(x_i^2 + y_i^2)\right] dP(U_x)dP(U_y) \tag{A.6}$$

$$dP(U_x)dP(U_y) = \frac{1}{(2\pi)^N \mid C \mid} \exp\left[-\frac{1}{2}\sum_{i,j=1}^{N} C^{-1}(x_ix_j + y_iy_j)dU_xdU_y\right]. \tag{A.7}$$

Rewriting eqn A.6 with Λ gives $L(s)$ as

$$L(s) = \frac{1}{(1+s)^N}\Lambda, \tag{A.8}$$

where

$$\Lambda = \frac{1}{(2\pi)^N \mid C \mid} \int\int \exp\left[-\frac{1}{2}\sum_{i,j=1}^{N} C^{-1}(x_ix_j + y_iy_j)\right.$$
$$\left. -\sum_{i=1}^{N} \frac{s}{1+s}(x_i^2 + y_i^2)\right] dU_xdU_y \tag{A.9}$$

Equation A.8 can be further simplified if we define the matrixes $\Psi(s)$ and $\Gamma(s)$ by

$$\Psi(s) \doteq \begin{cases} C^{-1}, & i \neq j \\ C^{-1} + \frac{2s}{1+s}, & i = j \end{cases}, \tag{A.10}$$

and

$$\Gamma(s) \doteq \mid \Psi(s) \mid. \tag{A.11}$$

Substituting in the above results, eqn A.9 is reduces to

$$
\Lambda \cdot \left[\frac{\Gamma(0)}{\Gamma(s)}\right] \left(\frac{\Gamma(s)}{(2\pi)^N} \int \int \exp\left[-\frac{1}{2}\sum_{i,j=1}^{N} \Psi(s)(x_i x_j + y_i y_j)\right] dU_x dU_y\right). \tag{A.12}
$$

The term in the parenthesis of eqn A.12 is just the integral of the pdf, which equals one. Thus, $L(s)$ reduces to

$$
L(s) = \frac{1}{(1+s)^N}\left[\frac{\Gamma(0)}{\Gamma(s)}\right]. \tag{A.13}
$$

Equation A.13 can also be expressed in terms of the eigenvalues of $\Psi(s)$ and the eigenvalues of the inverse signal covariance matrix, λ_i', where

$$
\lambda_i'(s) = \lambda_i' + \frac{2s}{1+s}; \tag{A.14}
$$

and

$$
\Gamma(0) = \prod_{i=1}^{N} \lambda_i' \tag{A.15}
$$

$$
\Gamma(s) = \prod_{i=1}^{N} \left(\lambda_i' + \frac{2s}{1+s}\right). \tag{A.16}
$$

Substituting in the above results gives the simplified form of $L(s)$:

$$
L(s) = \frac{1}{(1+s)^N} \prod_{i=1}^{N} \left[1 + \frac{2s}{(1+s)\lambda_i'}\right]^{-1} \tag{A.17}
$$

Equation A.17 can also be expressed in terms of the normalized signal covariance matrix eigenvalues if the following substitution is made for λ_i':

$$
\lambda_i' \doteq \frac{2}{\chi \lambda_i}. \tag{A.18}
$$

After some minor simplifications, eqn A.17 is given as:

$$L(s) = \prod_{i=1}^{N} \frac{1}{1 + s(1 + \chi \lambda_i)} \qquad (A.19)$$

The P_D is then determined by taking the inverse Laplace transform of eqn A.19 and integrating the resultant pdf from the threshold, V_T to infinity.

Appendix B. *Determination of the Exponential Covariance Matrix Eigenvalues*

The following method of calculating the eigenvalues for an exponential covariance matrix is taken from Irving Kanter's (14) paper on the detection of the correlated radar returns. It is included, because it provides an effective method from calculating the eigenvalues of large matrixes.

First consider the general case where the correlation of noncontiguous pulses may not be neglected. Recall that the eigenvalues of the full C matrix are required to calculate the P_D. The earlier results of chapter 2 neglected the noncontiguous pulses, which made the corresponding signal covariance matrix tridiagonal. The solution of the matrix equation was simplified through the use of the tridiagonal matrix. The same approach for determining the matrix eigenvalues can be used if the signal matrix can be made tridiagonal. This is easily done by noting that the inverse of the signal covariance matrix, C^{-1}, is a tridiagonal matrix. This inverse matrix can be written as

$$C^{-1} = \frac{1}{1-\rho^2} \begin{bmatrix} 1 & -\rho & 0 & \cdots & & 0 \\ -\rho & 1+\rho^2 & -\rho & 0 & & \vdots \\ 0 & \ddots & \ddots & \ddots & & 0 \\ \vdots & \ddots & & \ddots & 1+\rho^2 & -\rho \\ 0 & \cdots & & 0 & -\rho & 1 \end{bmatrix}. \tag{B.1}$$

The original matrix equation to be solved is

$$[C - \lambda I]U = 0 \tag{B.2}$$

which can be rewritten for the tridiagonal inverse matrix as

$$(1 - \rho^2) \left(C^{-1} - \frac{1}{\lambda} I \right) V = 0 \tag{B.3}$$

Recall the sum of the eigenvalues equals the trace of C giving the relation

$$\sum_{n=1}^{N} \lambda_n = N. \tag{B.4}$$

The equivalent homogeneous boundary value problem can be written as a set of homogeneous second order difference equations

$$- \rho v_{n-1} + \left(1 + \rho^2 - \frac{1 - \rho^2}{\lambda} \right) v_n - \rho v_{n+1} = 0, \qquad n = 1, \cdots, N \tag{B.5}$$

with the boundary conditions

$$\begin{aligned} v_0 - \rho v_1 &= 0 \\ v_{N+1} - \rho v_N &= 0 \end{aligned} \tag{B.6}$$

Since the equation is linear and has constant coefficients, there are two solution in the form of

$$v_n = \gamma^n \tag{B.7}$$

where γ is given as

$$\gamma = 1 + \rho^2 - \frac{1 - \rho^2}{\lambda} \pm \frac{\sqrt{\left(1 + \rho^2 - \frac{1 - \rho^2}{\lambda} \right)^2 - 4\rho^2}^{1/2}}{2\rho} \tag{B.8}$$

The condition

$$\mid (1 + \rho^2 - (1 - \rho^2)/\lambda)/(2\rho) \mid \geq 1 \tag{B.9}$$

implies either $\lambda \geq (1+\rho)/(1-\rho)$ or $\lambda \leq (1-\rho)/(1+\rho)$ eqn B.4 cannot be satisfied. Thus, we introduce the real angle θ by

$$\cos\theta \doteq \frac{1+\rho^2 - \frac{1-\rho^2}{\lambda}}{2\rho}, \tag{B.10}$$

and write the solution in the form of eqn 2.24. Application of the boundary conditions then yields the equations

$$[1 - \rho\cos\theta]K_1 - [\rho\sin\theta]K_2 = 0 \tag{B.11}$$

$$[\cos(N+1)\theta - \rho\cos N\theta]K_1 + [\sin(N+1)\theta - \rho\sin N\theta]K_2 = 0 \tag{B.12}$$

whose determinant must vanish. Thus, θ obeys the transcendental equation

$$\sin(N+1)\theta - 2\rho\sin N\theta + \rho^2\sin(N-1)\theta = 0. \tag{B.13}$$

Since the values $\theta = 0, \pi$ do not permit a nontrivial solution to the boundary value problem, the roots of eqn B.13 again line in the open interval $(0, \pi)$. Since it has not been possible to solve eqn B.13 analytically, the following remarks allow a numerical solution to be easily achieved: To show that there are exactly N roots between 0 and π, we first write as

$$[(1+\rho^2)\cos\theta - 2\rho]\sin N\theta + [(1-\rho^2)\sin\theta]\cos N\theta = 0 \tag{B.14}$$

and then introduce the function $\phi(\theta)$ by means of

$$\sin\phi(\theta) \doteq \frac{(1-\rho^2)\sin\theta}{1+\rho^2 - 2\rho\cos\theta} \tag{B.15}$$

$$\cos\phi(\theta) \doteq \frac{(1+\rho^2)\cos\theta - 2\rho}{1+\rho^2 - 2\rho\cos\theta} \tag{B.16}$$

so that eqn B.14 becomes

$$\sin[N\theta + \phi(\theta)] = 0. \qquad (B.17)$$

The derivative of ϕ with respect to θ yields the condition:

$$\frac{d\phi}{d\theta} = \frac{1 - \rho^2}{1 + \rho^2 - 2\rho\cos\theta} > 0 \qquad (B.18)$$

$\phi(\pi)$ can then be expressed as:

$$\phi(\pi) = \phi(0) + \int_0^\pi \frac{1 - \rho^2}{1 + \rho^2 - 2\rho\cos\theta} d\theta = \pi \qquad (B.19)$$

Equation B.17 represents a modulated sinusoid whose total phase increases monotonically from 0 at $\theta = 0$ to $(N + 1)\pi$ at $\theta = \pi$, it has exactly N distinct zero crossings in the open interval $(0, \pi)$.

Further, since $d^2\phi/d\theta^2 < 0$ in $(0, \pi)$ and $d\phi/d\theta = 1$ at $\cos\theta = \rho$, the function $\sin[N\theta + \phi(\theta)]$ oscillates more rapidly than does $\sin(N + 1)\theta$ in the domain $0 < \theta < \cos^{-1}\rho$ and more slowly (but still more rapidly than does $\sin(N\theta)$ in the domain $\cos^{-1}\rho < \theta < \pi$. Using these observations concerning the spacing of the roots, it is an easy matter to accurately locate the roots by means of a Newton-Raphson method.

Denoting the roots by $\theta_1, \cdots, \theta_N$ the eigenvalues are given by

$$\frac{1 - \rho}{1 + \rho} < \lambda_n = \frac{1 - \rho^2}{1 + \rho^2 - 2\rho\cos\theta_n} < \frac{1 + \rho}{1 - \rho} \qquad (B.20)$$

Note that the expansion of eqn B.20 into a power series in ρ yields a first order approximation which is identical to eqn 2.27.

Bibliography

1. Barton, D.K. and H.R. Ward. *Handbook of Radar Measurement*, chapter 6, 163–182. Artec House, Inc, 1984.

2. Blake, Lamont V. *Radar Range-Performance Analysis*, chapter 1, 100–200. Artec House, Inc, 1986.

3. Crispen, J.W. and K.M. Siegel. *Methods of Radar Cross-Section Analysis*. Academic Press, 1968.

4. Davenport, Wilbur B. Jr. *Probability and Random Processes*. McGraw-Hill Book Co., 1987.

5. Difranco, J.V. and W. L. Rubin. *Radar Detection*, chapter 11, 373–445. Artec House, Inc, 1980.

6. Difranco, J.V. and W. L. Rubin. *Radar Detection*, chapter 10, 364–371. Artec House, Inc, 1980.

7. Edrington, T. S. "The Amplitude Statistics of Aircraft Radar Echoes," *IEEE Transactions on Military Electronics*, 9:10–16 (January 1965).

8. Haykin, Simon S. *Detection and Estimation. Application to Radar*, chapter 1, 0–300. Dowden, Hutchinson, and Ross, Inc., 1976.

9. Helstrom, C. W. and J. A. Ritcey. "Evaluating radar detection probabilities by steepest descent integration," *IEEE Transactions on Aerospace and Electronic Systems*, AES(20):624–634 (September 1984).

10. Helstrom, Carl W. "Approximate evaluation of detection probabilities in radar and optical communications," *IEEE Transactions on Aerospace and Electronic Systems*, AES(14):630–640 (July 1978).

11. Helstrom, Carl W. "Evaluating the detectability of Gaussian stochastic signals by steepest descent integration," *IEEE Transactions on Aerospace and Electronic Systems*, AES(19):428–437 (May 1983).

12. Helstrom, Carl W. "Detection Probabilities for Correlated Rayleigh Fading Signals," *IEEE Transactions on Aerospace and Electronic Systems*, 28(1):259–267 (January 1992).

13. IMSL Problem-Solving Software Systems. "User's Manual Math/Library FORTRAN Subroutines for Mathematical Applications,". Houston, Texax, 1987.

14. Kanter, Irving. "Exact Detection Probability for Partially Correlated Rayleigh Targets." *IEEE Transaction on Aerospace and Electronic Systems*, 22(2):184–195 (March 1986).

15. Levanon, Nadav. *Radar Principles*, chapter 2, 0–300. John Wiley and Sons, Inc., 1988.

16. Schwartz, Mischa. "Effects of Signal Fluctuation on the Detection of Pulse Signals in Noise," *IRE Transactions on Information Theory*, 66–71 (June 1956).

17. Skolnik, Merrill I. *Introduction to Radar Systems*. New York: McGraw-Hill Book Company, 1980.

18. Swerling, Peter. "Detection of Fluctuating Pulsed Signals in the Presence of Noise," *IRE Transaction on Information Theory*, 175–178 (September 1957).

19. Swerling, Peter. "Probability of Detection for Fluctuating Targets," *IRE Transaction on Information Theory*, IT(6):273–308 (April 1960).

20. Welsh Byron, Joseph Phillip and Pyati Vittal. "RCS Autocovariance Functions and Power Spectral Densities of Complex Targets." Unpublished report, Air Force Institute of Technology, 1991.

Vita

Alan L. Buterbaugh was born on 4 June 1959 in Warren, Ohio. In 1977, he graduated from Southeast High School and enlisted in the United States Air Force. While enlisted, he served as an Avionics Sensor Systems Technician for the Tactical Air Command. In 1985, he received a Bachelor of Science in Electrical Engineering from The University of Akron. After receiving his commission at The University of Akron in 1985, he was assigned to the Aeronautical Systems Division, Wright-Patterson AFB, where he worked as a Low Observables engineer for the B-2 Special Program Office. He was selected in January 1991 to attend the School of Engineering, Air Force Institute of Technology.

Permanent address: 7947 Newton Falls Rd
Ravenna, OH 44266

REPORT DOCUMENTATION PAGE

Public reporting burden for this collection of information is estimated to average 1 hour per response, including the time for reviewing instructions, searching existing data sources, gathering and maintaining the data needed, and completing and reviewing the collection of information. Send comments regarding this burden estimate or any other aspect of this collection of information, including suggestions for reducing this burden, to Washington Headquarters Services, Directorate for Information Operations and Reports, 1215 Jefferson Davis Highway, Suite 1204, Arlington, VA 22202-4302, and to the Office of Management and Budget, Paperwork Reduction Project (0704-0188), Washington, DC 20503.

1. AGENCY USE ONLY (Leave blank)	2. REPORT DATE September 1992	3. REPORT TYPE AND DATES COVERED Master's Thesis

4. TITLE AND SUBTITLE
The Detection and Correlation Modeling
of Rayleigh Distributed Radar Signals

5. FUNDING NUMBERS

6. AUTHOR(S)
Alan L. Buterbaugh

7. PERFORMING ORGANIZATION NAME(S) AND ADDRESS(ES)
Air Force Institute of Technology, WPAFB OH 45433-6583

8. PERFORMING ORGANIZATION REPORT NUMBER
AFIT/GE/ENG/92S-03

9. SPONSORING / MONITORING AGENCY NAME(S) AND ADDRESS(ES)
Capt Pete Collins
6585 Test Group
Radar Scatterer Div
Holloman AFB NM 88330-5000

10. SPONSORING / MONITORING AGENCY REPORT NUMBER

11. SUPPLEMENTARY NOTES

12a. DISTRIBUTION / AVAILABILITY STATEMENT

Distribution Unlimited

12b. DISTRIBUTION CODE

13. ABSTRACT (Maximum 200 words)

Abstract

This thesis provides a method for determining the detection of partially correlated Rayleigh distributed radar returns by a pulsed search radar. The receiver consists of a quadrature demodulator receiver, followed by a square law envelope detector and a linear post-detection integrator. In addition, a technique for determining the pulse-to-pulse correlation of a complex target is given using inverse Fourier transforms of the target scattering centers. An AIM-9 missile is used to illustrate how the partially correlated detection techniques and the pulse-to-pulse correlation predictions can be used to determine the probability of detection.

14. SUBJECT TERMS
The Detection and Correlation Modeling of Rayleigh Distributed Radar Signals

15. NUMBER OF PAGES
78

16. PRICE CODE

17. SECURITY CLASSIFICATION OF REPORT	18. SECURITY CLASSIFICATION OF THIS PAGE	19. SECURITY CLASSIFICATION OF ABSTRACT	20. LIMITATION OF ABSTRACT
UNCLASSIFIED	UNCLASSIFIED	UNCLASSIFIED	UL